Journal of the American Heart Association

ORIGINAL RESEARCH

Protective Role of Endothelial Fibulin-4 in Valvulo-Arterial Integrity

Tram Anh Vu Nguyen, BS; Caroline Antunes Lino, PhD; Huynh Thuy Hang, MS; Juliano Vilela Alves, MS; Bui Quoc Thang, MD, PhD; Seung Jae Shin, PhD; Kaori Sugiyama, PhD; Hiroko Matsunaga, PhD; Haruko Takeyama, PhD; Yoshito Yamashiro, PhD; Hiromi Yanagisawa, MD, PhD

BACKGROUND: Homeostasis of the vessel wall is cooperatively maintained by endothelial cells (ECs), smooth muscle cells, and adventitial fibroblasts. The genetic deletion of fibulin-4 (*Fbln4*) in smooth muscle cells (*SMKO*) leads to the formation of thoracic aortic aneurysms with the disruption of elastic fibers. Although *Fbln4* is expressed in the entire vessel wall, its function in ECs and relevance to the maintenance of valvulo-arterial integrity are not fully understood.

METHODS AND RESULTS: Gene silencing of *FBLN4* was conducted on human aortic ECs to evaluate morphological changes and gene expression profile. *Fbln4* double knockout (*DKO*) mice in ECs and smooth muscle cells were generated and subjected to histological analysis, echocardiography, Western blotting, RNA sequencing, and immunostaining. An evaluation of the thoracic aortic aneurysm phenotype and screening of altered signaling pathways were performed. Knockdown of *FBLN4* in human aortic ECs induced mesenchymal cell–like changes with the upregulation of mesenchymal genes, including *TAGLN* and *MYL9*. *DKO* mice showed the exacerbation of thoracic aortic aneurysms when compared with those of *SMKO* and upregulated Thbs1, a mechanical stress–responsive molecule, throughout the aorta. *DKO* mice also showed progressive aortic valve thickening with collagen deposition from postnatal day 14, as well as turbulent flow in the ascending aorta. Furthermore, RNA sequencing and immunostaining of the aortic valve revealed the upregulation of genes involved in endothelial-to-mesenchymal transition, inflammatory response, and tissue fibrosis in *DKO* valves and the presence of activated valve interstitial cells.

CONCLUSIONS: The current study uncovers the pivotal role of endothelial fibulin-4 in the maintenance of valvulo-arterial integrity, which influences thoracic aortic aneurysm progression.

Key Words: aneurysm ■ aortic valve ■ endothelial cells ■ fibulin-4 ■ smooth muscle cells

Thoracic aortic aneurysm (TAA) refers to an irreversible enlargement of the aortic wall that exceeds 1.5 times the normal aortic diameter. TAAs typically progress asymptomatically and can be life-threatening when they rupture or dissect.[1] Surgical resection or stent graft insertion is commonly performed as a prophylactic measure against aortic rupture; however, effective medications to halt or reverse TAA progression have yet to be established.[2] TAAs can be associated with heritable diseases with syndromic features, (eg, Marfan syndrome and Loeys-Dietz syndrome) and exhibit the marked activation of transforming growth factor β (TGF-β) and mitogen-activated protein kinase signaling in vascular smooth muscle cells (SMCs).[3,4] Mutations in extracellular matrix (ECM) proteins and SMC contractile proteins are also related to the development of TAAs.[5,6] On this basis, therapeutic strategies targeting SMCs with angiotensin type 1 receptors have been developed; however, their efficacy over conventional medications (eg, β-blockers) has not been confirmed in human patients.[7,8] More recently, the contribution of vascular endothelial cells (ECs) has been reported as a crucial factor in TAA

Correspondence to: Yoshito Yamashiro, PhD, Laboratory Chief Department of Advanced Medical Technologies, National Cerebral and Cardiovascular Center Research Institute, Osaka 564-8565, Japan. Email: yamayoshito@ncvc.go.jp
Hiromi Yanagisawa, MD, PhD, Professor Life Science Center for Survival Dynamics, Tsukuba Advanced Research Alliance University of Tsukuba, Ibaraki 305-8577, Japan. Email: hkyanagisawa@tara.tsukuba.ac.jp

Supplemental Material is available at https://www.ahajournals.org/doi/suppl/10.1161/JAHA.122.026942

For Sources of Funding and Disclosures, see page 13.

JAHA is available at: www.ahajournals.org/journal/jaha

CLINICAL PERSPECTIVE

What Is New?

- Generation of endothelial cell– and smooth muscle cell–specific double knockout mice for fibulin-4 reveals that fibulin-4 is essential for maintaining valvulo-arterial integrity, which serves a critical role in preventing the progression of aneurysm expansion.
- Double knockout mice exhibit abnormal thickening of the aortic valves with altered transcriptome profiles suggestive of endothelial-to-mesenchymal transition.

What Are the Clinical Implications?

- The current study provides in vivo evidence for the pathological interactions of aortic valve abnormality and aortopathy that synergistically exacerbate thoracic aortic aneurysms.
- Routine monitoring and assessment of the aortic valve functions in patients with thoracic aortic aneurysms are helpful for the prediction of clinical outcomes for thoracic aortic aneurysm.

Nonstandard Abbreviations and Acronyms

α-SMA	α-smooth muscle actin
DKO	double knockout
EC	endothelial cell
ECKO	endothelial cell-specific knockout
ECM	extracellular matrix
Egr1	early growth response 1
EndMT	endothelial-to-mesenchymal transition
Fbln4	fibulin-4
Gdf15	growth differentiation factor-15
HAEC	human aortic endothelial cell
RNA-seq	RNA sequencing
SMC	smooth muscle cell
SMKO	smooth muscle cell-specific knockout
TAA	thoracic aortic aneurysm
TGF-β	transforming growth factor β
Thbs1	thrombospondin-1
VIC	valve interstitial cell

pathogenesis. For example, the endothelial angiotensin type 1 receptor is responsible for aneurysm formation in *Fbn1*$^{mgR/mgR}$ mice,[9] while endothelial ADAM17 contributes to elastase-induced TAAs by disrupting endothelial junctions.[10] Additionally, endothelial ROBO4 mutation or deficiency in mice results in TAA formation with a bicuspid aortic valve.[11] A bicuspid aortic valve is associated with TAAs in humans,[12] which demonstrates the involvement of multiple cell types in TAA. However, how these cells interact and influence the formation of TAAs is not completely understood.

In previous research, we developed a mouse model of postnatal TAA using the SMC-specific deletion of the *Efemp2* gene, which encodes extracellular matrix fibulin-4 (*Fbln4*^{SMKO}, termed *SMKO*).[13] Fibulin-4 localizes on microfibrils and is involved in the formation of elastic fibers. It is expressed throughout the entire vessel wall, including in ECs, SMCs, and adventitial fibroblasts, with the total deletion of fibulin-4 (*Fbln4*) resulting in neonatal death caused by aortic rupture.[14] In *SMKO* mice, pathological changes—including the focal accumulation of dedifferentiated SMCs—were observed in the ascending aorta from postnatal day 7 (P7), and enlargement of the aorta was evident at approximately P14.[15] The disruption of elastic fibers and its connection to SMCs leads to the upregulation of mechanical stress–responsive molecules, including protease-activated receptor 1, early growth response 1 (Egr1), angiotensin-converting enzyme, and thrombospondin-1 (Thbs1), thereby generating a feed-forward loop of the mechanical stress–induced activation of proteases and angiotensin II–mediated signaling in the aortic wall. Additionally, an increased abundance of the cytoskeletal regulators slingshot 1 (Ssh1) and cofilin results in an excess of globular actin, which compromises the integrity of the aortic wall.[15–18] Although the pharmacological inhibition of angiotensin type 1 receptor by losartan and the genetic deletion of *Thbs1* largely prevented the formation of TAA in *SMKO* mice,[15,17] cell type–specific function of *Fbln4* in aneurysm development is still unknown.

In this study, we used mice with the EC-specific deletion of *Fbln4* (*Fbln4*^{ECKO}) to generate EC and SMC double knockout mice for *Fbln4* (*Fbln4*$^{ECKO;SMKO}$, termed *DKO*) and also investigated the endothelial contribution of fibulin-4 in TAA formation. We found that *DKO* mice exacerbated aortic aneurysms with the activation of cardiac valve interstitial cells (VICs) and thickened aortic valves accompanied by turbulent aortic blood flow. Finally, transcriptome analysis detected critical molecules involved in abnormal valvular changes, which revealed the protective role of fibulin-4 in valvulo-arterial homeostasis.

METHODS

Detailed descriptions are provided in Data S1. All data supporting the findings of this study are available from the corresponding authors upon reasonable request.

Mice

SMC-specific *Fbln4* knockout mice (*Fbln4*$^{loxP/KO}$; SM22α-Cre, *SMKO*) and EC-specific *Fbln4* knockout

mice (*Fbln4*$^{loxP/KO}$; Tie2-Cre, *ECKO*) were generated as previously described.[13] These were mated to generate double knockout mice for *Fbln4* in SMCs and ECs (*Fbln4*$^{ECKO/SMKO}$, *DKO*). *Fbln4*$^{+/+}$ or *Fbln4*$^{loxp/+}$ mice containing the SM22α-Cre or Tie2-Cre transgenes were used as controls in this study (Table S1). Phenotypic comparisons were performed between animals (the number of animals is indicated in each figure legend) with the same genetic background, and both males and females (approximately 1:1 ratio) were used in the study. There were no phenotypic differences in aneurysm formation and incidence between males and females. All mice were kept on a 12 hour/12 hour light/dark cycle under specific pathogen-free conditions and all animal protocols were approved by the Institutional Animal Experiment Committee of the University of Tsukuba (APN: 21–108 and 22–294).

Genotyping

Mouse DNA was collected from ear samples and extracted by Hotshot methods as previously described.[13] Briefly, ear samples were heated with alkaline lysis reagent (25 mM NaOH, 0.2 mM EDTA, pH12.0) at 95°C for 30 minutes and stored at 4°C. Neutralization reagents (40 mM Tris–HCl, pH5.0) were added and mixed well. Subsequent genotyping was performed using GoTaq green master mix (Promega) and specific primers (Table S2).

Cell Culture, siRNA Transfection, and RNA Sequencing

Human aortic ECs (HAECs; Lonza, CC-2535; lot#18TL099141 and 18TL177324) passages between 6 and 10 were grown in EGM-2 BulletKit (Lonza, CC-3162) supplemented with 2% (v/v) fetal bovine serum and growth factors. HAECs were transiently transfected with 10 pmol for a final concentration of scramble (nontarget) small interfering RNA (siRNA) (Invitrogen, #12935110) and *FBLN4*-siRNA (EFEMP2HSS121198) using lipofectamine RNAiMAX transfection reagent (Thermo Fisher Scientific, #13778075) according to the manufacturer's instructions. After 4 days of transfection, total RNA was extracted using an RNeasy mini kit (QIAGEN) according to the manufacturer's protocol, and RNA concentration was quantified by Nanodrop One (Thermo Fisher). Total RNA (500 ng) was used for RNA-sequencing (RNA-seq) library preparation, and sequencing was performed by Azenta Japan Corp. using NovaSeq/HiSeq (Illumina). FASTQ files were analyzed using CLC Genomics Workbench (version 22.0, QIAGEN). Sequences were mapped to the human genome (GRCh38.105), and annotated genes were quantified using CLC Genomics Workbench.

Western Blot Analysis

At 2 to 4 months old, aortas were harvested without perivascular adipose tissues. Aortas were then minced in liquid nitrogen by a pestle and dissolved in RIPA lysis buffer (Sigma-Aldrich, R0278) containing 1% of protease inhibitor (Sigma-Aldrich, P8340) and 1% of phosphatase inhibitor (Wako, #167-24381), as previously described.[3] Total proteins were mixed with 3 × SDS sample buffer containing 2-mercaptoethanol, boiled at 95°C for 5 minutes, and then proceeded for SDS-polyacrylamide gel electrophoresis. Proteins were transferred to a polyvinylidene difluoride (PVDF) membrane (Millipore, IPVH00010), blocked, and immunoblotted with the primary antibodies indicated in Table S3. Membranes were then incubated with respective anti-mouse (Bio-Rad, #170–6516) or anti-rabbit HRP-conjugated secondary antibodies (1:1000, Bio-Rad, #170–6515) for 1 hour at room temperature and visualized using a chemiluminescence kit (Santa Cruz Biotechnology, sc-2048) or SuperSignal West Femto Maximum Sensitivity Substrate (Thermo Fisher Scientific, #34094). GAPDH was used as an internal control. X-ray film and an automatic X-ray processor machine (FUJIFILM, FPM100) were used for detection.

Immunostaining of Mouse Aortas and Aortic Valves

For immunostaining, 10-μm cross-sections of the mouse aorta and aortic valves were immediately fixed with 4% paraformaldehyde for 30 minutes, washed twice with 1 × PBS, then blocked in 5% bovine serum in which secondary antibodies were raised (containing 0.1% Tween-20) for 1 hour at room temperature. The primary antibodies used are shown in Table S3. Incubation was performed overnight at 4°C. After washing, highly cross-absorbed Alexa Fluor 546- or 647-conjugated secondary antibodies (Invitrogen and Jackson ImmunoResearch) were added at a dilution of 1:200 or 1:400 for 1 to 2 hours at room temperature. Control experiments were performed by omitting the primary antibody. Slides were covered with Vectashield containing DAPI (Vector Laboratories, H-1200) or counterstained nuclear by Hoechst at 1:1000 dilution with secondary antibodies, then mounted with SlowFade Diamond Antifade Mountant (Invitrogen, S36972) and viewed under an LSM 710 microscope (ZEISS). Fluorescence intensity was measured by ImageJ software (National Institutes of Health).

Statistical Analysis

Prism 8 (GraphPad, version 8.4.2) was used for statistical analysis. Shapiro–Wilk test was used for the normality test. When the data followed a normal distribution, statistical significance was determined by 1-way ANOVA and post hoc Tukey multiple comparisons test. The graphs are presented as the mean ± SEM. If the normality assumption was violated, nonparametric

tests (ie, a Kruskal-Wallis test with Dunn multiple comparisons) were conducted. Kruskal-Wallis test was used in Figure 3B (for pSmad2/Smad2/3), Figure 4A, and Figure S1 and S2B (for Thbs1 and decapentaplegic homolog 2 extracellular signal-regulated kinase/extracellular signal-regulated kinase). The graphs are presented as median with interquartile range or minimum to maximum range, with *P<0.05, **P<0.01, and ***P<0.001 denoting statistical significance.

Data Availability

RNA-seq data have been deposited in the Gene Expression Omnibus (GEO) database, http://www.ncbi.nlm.nih.gov/geo/. The accession number is GSE204771 for HAECs (Figure 1) and GSE204772 for aortic valves (Figure 6).

RESULTS

Fbln4 Knockdown Induces Phenotypic Changes in ECs

Although Fbln4 is expressed throughout the aortic wall, its in vivo deletion in ECs alone (*ECKO*) does not result in aortic aneurysms.[13] Because Fbln4 is locally produced by SMCs and is detected in plasma,[19] the absence of the aortic phenotype in *ECKO* is likely caused by the compensation from other cell sources. To examine whether *FBLN4* deletion induces the alteration of endothelial phenotypes, we knocked down *FBLN4* in HAECs using *FBLN4* siRNA. Compared with scramble siRNA-treated control cells that exhibited a typical small and round cobblestone-like morphology, *Fbln4* knockdown cells (si*FBLN4*) were flattened, elongated, and showed a mesenchymal-like appearance (Figure 1A). RNA-seq followed by principal component analysis clearly separated the si*FBLN4* group from the scramble siRNA-treated control cells group (Figure 1B). Gene ontology enrichment analyses revealed that genes involved in the immune system, ECM organization, and neutrophil degradation were highly enriched in si*FBLN4* (Figure 1C). Furthermore, transcriptional regulatory relationships unraveled by sentence-based text-mining analysis showed that transcription factors involved in the regulation of EC proliferation (*SP1*, *STAT3*, *STAT1*, *TWIST1*, *ETS1*, *KLF4*) and response to SMC stretch (*JUN*, *RELA*, *NFKB1*, *SRF*, *EGR1*) were enriched in si*FBLN4*. Interestingly, *ADAMTS1*—an ECM protease involved in TAA[20,21]—was most heavily downregulated in si*FBLN4* together with *MMP1*, *ADAMTS9*, and *ADAMTS18*. Conversely, SMC genes such as *TGLN* and *MYL9*, and interferon-induced genes such as *IFIT1* and *IFITM1*, were upregulated in si*FBLN4* (Figure 1D). These results suggest that the loss of *Fbln4* alters the EC phenotype and the expression of genes involved in vascular homeostasis.

Deletion of Fbln4 in ECs and SMCs Exacerbates Thoracic Aortic Aneurysm

To examine the function of fibulin-4 in ECs in vivo and determine its relevance to TAA formation, we crossed *ECKO* with *SMKO* mice to obtain EC and SMC *DKO* mice. The generation of *DKO* mice was confirmed by genomic polymerase chain reaction (Figure 2A and Table S1), and aneurysms were examined at 2 months old and compared with respective control, *ECKO*, and *SMKO* littermates. The aortic diameter was increased in *SMKO* and *DKO* mice during diastole and systole, as measured by echocardiography (Figure S1). Consistent with previous reports, *SMKO* mice only developed aortic aneurysms in the ascending region, whereas *DKO* mice developed more severe TAAs that enlarged from the aortic arch to the left subclavian artery (Figure 2B, pink arrowhead). *DKO* mice also showed severe tortuosity in the descending aorta when compared with *SMKO* mice (Figure 2B, yellow arrowheads). In contrast, *ECKO* mice were comparable with control mice and did not show any vascular abnormalities (Figure 2B). Histologically, *ECKO* mice did not exhibit the proliferation of SMCs or disruption of elastic fibers as previously reported[13] (Figure 2C). Similar to *SMKO* mice, *DKO* mice showed a thickened aortic wall, disruption of elastic fibers, and collagen accumulation in the medial and adventitial layers. The disruption of elastic fibers was also confirmed using an electron microscope (Figure S1). Morphometric analysis indicated that the internal elastic lamina (IEL) perimeter, outer perimeter, wall thickness, and total vessel area were increased in *SMKO* and *DKO* mice when compared with control and *ECKO* mice; however, little difference was observed between the aortas of *SMKO* and *DKO* mice (Figure 2D). To evaluate the expansion of the aneurysmal area, we then examined the aneurysmal surface area in *SMKO* and *DKO* mice and compared it with that of control aortas. The thoracic aorta was opened longitudinally, and its surface area was measured from the aortic root to the branch of the left subclavian artery. A significant enlargement of the aneurysmal surface area was observed in *DKO* mice (average 34.50 mm^2) compared with control (average 7.41 mm^2) and *SMKO* (average 20.37 mm^2) mice, as shown in Figure 2E. Thus, *Fbln4* deficiency in ECs in vivo revealed a previously unrecognized role of endothelial Fbln4 in protecting the progression of aortic aneurysms in *SMKO* mice.

Aneurysmal Signaling Is Upregulated in the Ascending Aortas of *DKO* and *SMKO* Mice

To investigate the molecular signaling responsible for changes in *DKO* aortas, we performed Western blotting analysis to determine the levels of aneurysm-related

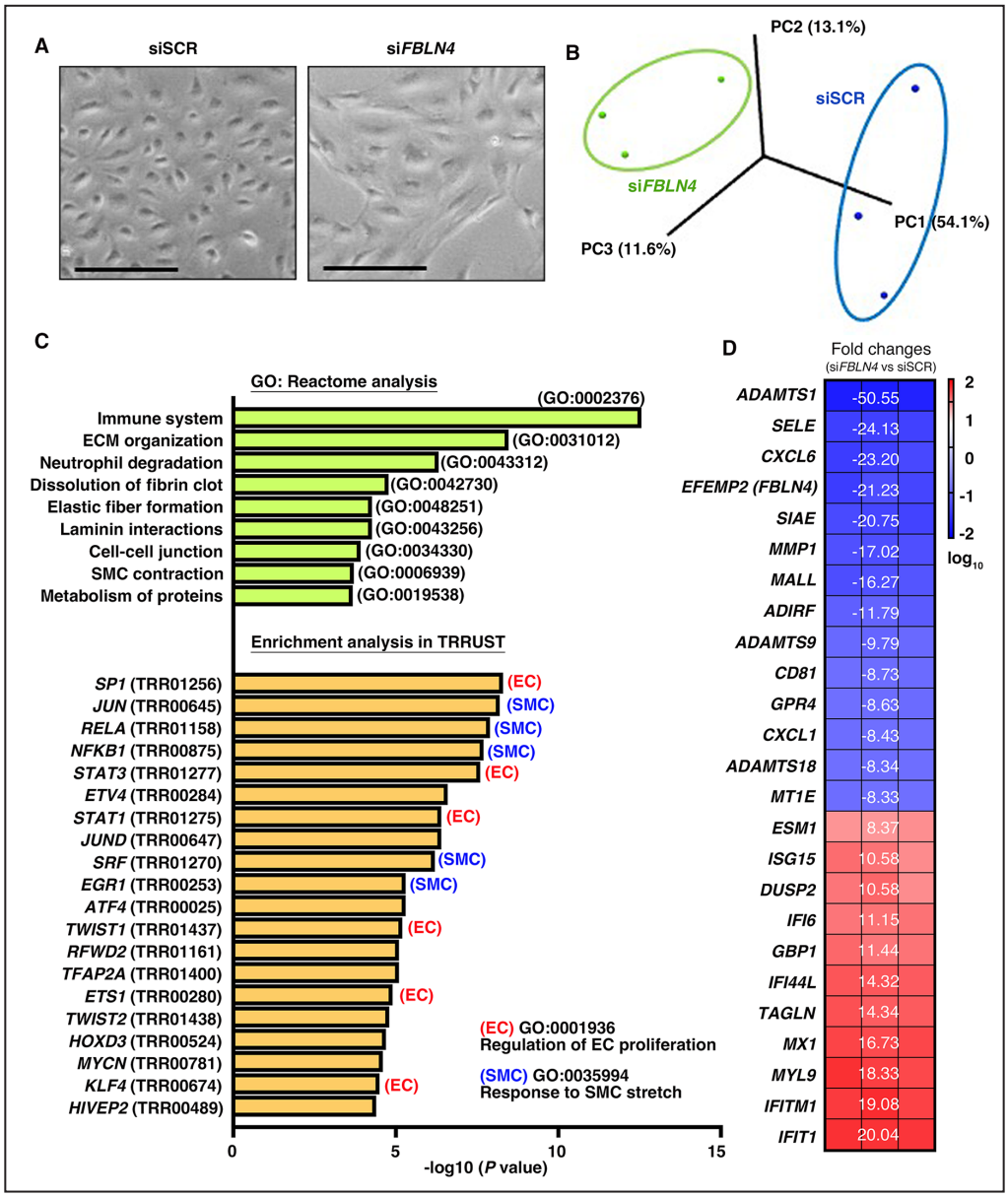

Figure 1. Molecular and phenotypic changes induced by *Fbln4* knockdown in ECs.
A, Cell morphology 4 days after transfection with nontargeted siSCR or si*FBLN4*. Scale bars are 200 μm. **B**, PC analysis plot shows distinct clusters between siSCR and si*FBLN4*. PC1 (54.1%), PC2 (13.1%), and PC3 (11.6%). **C**, List from gene ontology enrichment analysis (upper) and transcription factor-target interaction analysis by transcriptional regulatory relationships unraveled by sentence-based text-mining analysis (bottom). **D**, Heat map of top genes differentially expressed (fold changes >±8.0) between siSCR and si*FBLN4*. The $\log_{10}$ values from each experiment (n=3, per column) are shown in the heatmap. ECs indicates endothelial cells; *Fbln4*, fibulin-4; PC, principal component; si*FBLN4*, *FBLN4*-siRNA; siSCR, scramble RNA; and SMC, smooth muscle cell.

signaling molecules, including mechanical stress–responsive proteins previously identified in the *SMKO* aortas.[15–17] Angiotensin-converting enzyme, Thbs1, and Egr1 were significantly increased in the ascending aortas of both *SMKO* and *DKO* mice, whereas proto-oncogene tyrosine–protein kinase (Src) phosphorylation was most significantly increased in the *DKO* aortas (Figure 3). In contrast, the phosphorylation levels of decapentaplegic homolog 2 extracellular signal-regulated kinase were statistically unchanged among the 4 groups. In the descending aortas, Thbs1 was highly expressed only in the *DKO* mice, which is consistent with the aneurysmal expansion (Figure S2). Because EC defects have been shown to cause abnormal responses to flow-induced shear stress and increase EC permeability,[22] we then performed vascular permeability analysis to assess the

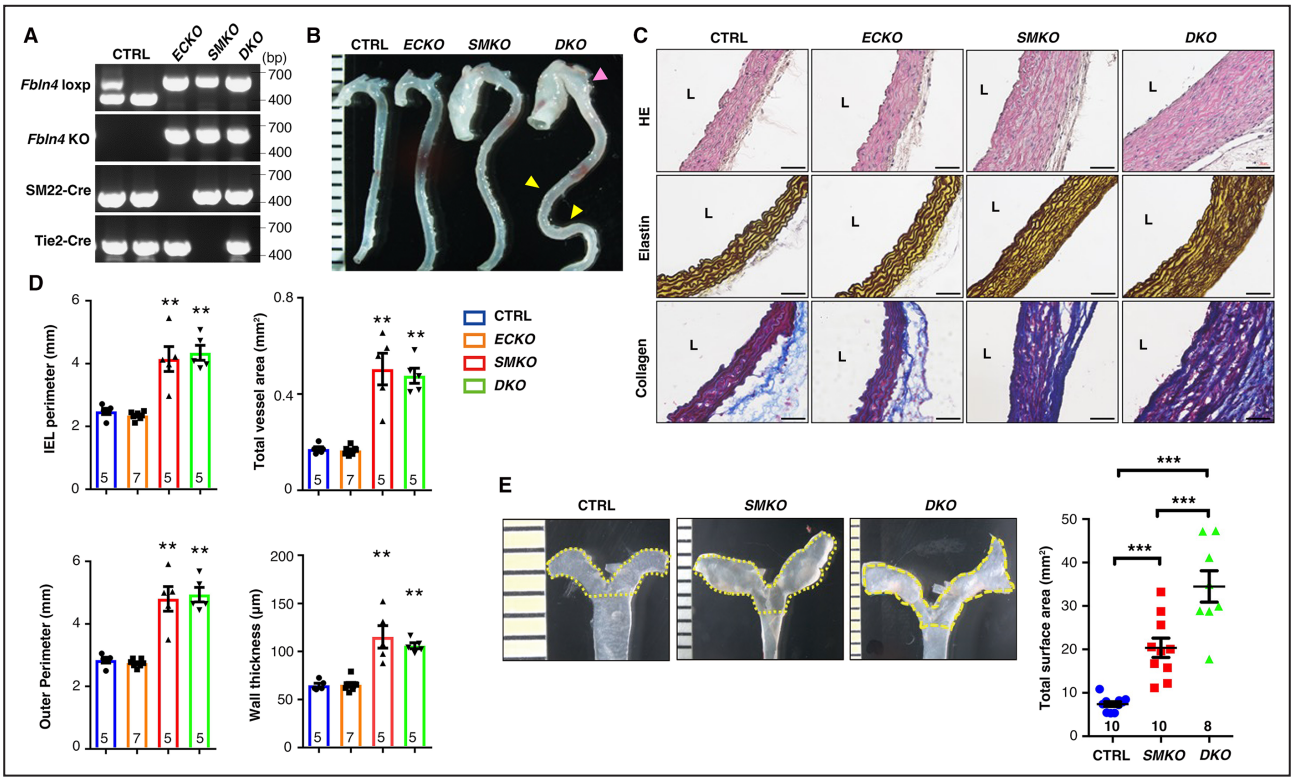

Figure 2. Loss of *Fbln4* in ECs and SMCs exacerbates aneurysm phenotype in mice.
A, Genomic polymerase chain reaction confirming the genotypes of mutant mice. *Fbln4* loxp: 670 bp, wild-type: 470 bp, KO: 540 bp, *SM22*-Cre: 500 bp, *Tie2*-Cre: 500 bp. **B**, Gross photos of CTRL, *ECKO*, *SMKO*, and *DKO* mice aortas at 2 months old. The pink arrowhead shows an expanded-aneurysm in a *DKO* aorta. Yellow arrowheads show severe tortuosity in *DKO* descending aorta. **C,** Histological images of cross-sections of the ascending aorta from 2-month-old CTRL (n=5), *ECKO* (n=7), *SMKO* (n=5), and *DKO* (n=5) mice stained with HE, Hart (elastin), and Masson trichrome (collagen). Scale bars are 50 μm. L; lumen. **D**, Morphometric analysis showing internal elastic lamina perimeter, outer perimeter, total vessel area, and wall thickness. CTRL (n=5), *ECKO* (n=7), *SMKO* (n=5), *DKO* (n=5) mice. Bars are means ± SEM. $^{**}P<0.01$, 1-way ANOVA. **E**, Gross photo of the longitudinally opened thoracic aorta. The yellow dotted line shows the total aneurysmal surface area. Quantification graph is shown on the right. CTRL (n=10), *SMKO* (n=10), and *DKO* (n=8). Bars are means ± SEM. $^{***}P<0.001$, 1-way ANOVA. CTRL indicates control; *DKO*, double knockout; ECs, endothelial cells; *ECKO*, endothelial cell-specific knockout; Fbln4, fibulin-4; HE, hematoxylin and eosin; KO, Fbln4 knockout; SMCs, smooth muscle cells; and *SMKO*, smooth muscle cell–specific knockout.

effect of *Fbln4* deficiency on EC function. Evans blue dye was injected through the tail vein, and leakage into the vessel wall was assessed after 1 hour (Figure S3A). Contrary to our prediction, no Evans blue leakage was observed into the medial layer of *ECKO* or *DKO* aortas (Figure S3B). Based on these results, it is unlikely that the damaged EC–cell junctions are the basis for the exacerbated aneurysm phenotype in *DKO* mice, which suggests that alternative or parallel mechanism(s) are involved in this process.

DKO Mice Showed Cardiac Hypertrophy and Turbulent Blood Flow

For our next experiments, we focused on evaluating cardiac functions and blood flow using color Doppler echocardiography. We observed cardiac hypertrophy in both *SMKO* and *DKO* mice at 2 months old. The ratio of heart weight to body weight was significantly increased in the *SMKO* (average 8.08 mg/g, median 7.60 mg/g) and *DKO* (average 9.14 mg/g, median 8.46 mg/g) mice when compared with control (average 6.21 mg/g, median 6.05 mg/g) and *ECKO* (average 6.26 mg/g, median 6.18 mg/g) mice (Figure 4A). Turbulent blood flow was also observed in *DKO* mice. Interestingly, the blood velocity waveforms showed reversed diastolic blood velocity in the ascending aortas of *DKO* mice, and concomitant antegrade (red) and retrograde (blue) flow velocities and turbulence (green and yellow) were evident with color Doppler (Figure 4B). Furthermore, morphometric analysis of the heart using M mode confirmed the hypertrophy of *DKO* mice (average 7.66 mg/g) because their left ventricular mass was higher than that of control (average 3.51 mg/g), *ECKO* (average 5.04 mg/g), and *SMKO* (average 4.88 mg/g) mice (Figure 4C). Despite this, no changes in cardiac functions (eg, ejection fraction and fractional shortening) were observed in *DKO* mice. Additionally, no

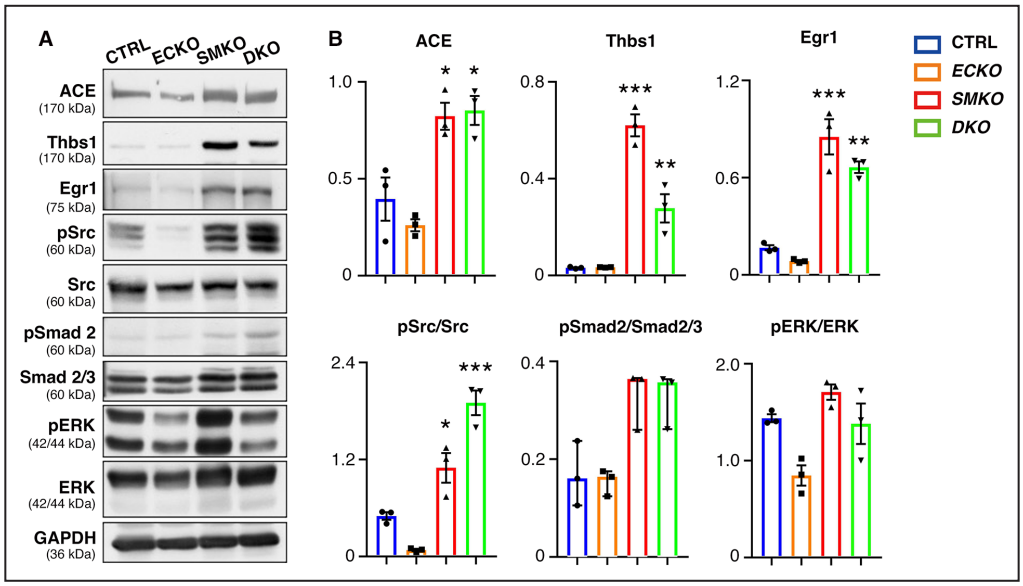

Figure 3. Aneurysmal signaling is upregulated in both *SMKO* and *DKO* ascending aorta.
A, Representative Western blots of ascending aorta from 2-month-old CTRL (n=3, pooled 3 aortas per group), *ECKO* (n=3, pooled 2 aortas per group), *SMKO* (n=3, one aorta per group), and *DKO* (n=3, pooled 2 aortas per group) mice. **B,** Quantification of Western blots is shown in the graphs. **P*<0.05, ***P*<0.01, ****P*<0.001, 1-way ANOVA for ACE, Thbs1, Egr1, pSrc, and pERK, bars are mean ± SEM. Kruskal-Wallis test for pSmad, bars are median with minimum to maximum range. ACE indicates angiotensin-converting enzyme; CTRL, control; *DKO*, double knockout; *ECKO*, endothelial cell–specific knockout; Egr1, early growth response 1; ERK, extracellular signal-regulated kinase; pERK, decapentaplegic homolog 2 extracellular signal-regulated kinase; pSmad, Smad phosphorylation; pSrc, Src phosphorylation; Smad, suppressor of mothers against decapentaplegic; *SMKO*, smooth muscle cell–specific knockout; Src, proto-oncogene tyrosine–protein kinase; and Thbs1, thrombospondin-1.

differences were observed between control, *ECKO*, *SMKO*, and *DKO* mice in the interventricular septum, left ventricular internal diameter, and left ventricular posterior wall during systole and diastole (Figure 4D). Consistent with echocardiography measurements, histological analysis of interventricular septum, left ventricular internal area, and left ventricular posterior wall in the heart cross-sections showed no differences among 4 genotypes at P60 (Figure S4). The cardiac functions were also maintained at 4 months old when the *DKO* mice showed a marked increase in the aortic diameter (Figure S5). These results indicate that cardiac hypertrophy and turbulent flow in *DKO* mice may be responsible for the more severe progression of aortic aneurysms.

DKO Mice Have Abnormal Aortic Valves From P14

The aortic valve is under constant mechanical stress (eg, shear stress and axial strain) and keeps unidirectional blood flow from the heart. Abnormalities in the morphology and function of the aortic valves are associated with cardiac hypertrophy and aortic aneurysms, and *Fbln4* hypomorphic mice (*Fbln4*$^{R/R}$) have been shown to develop thickening of the aortic valve.[23,24] We also observed the presence of aortic valve stenosis with increased aortic transvalvular systolic mean gradients and peak velocity as well as aortic valve insufficiency with reversed diastolic blood flow in *DKO* mice at 2 months old by pulse wave Doppler tracing of transvalvular flow velocity (Figure S6). To investigate the causal relationship between aortic valve abnormalities, cardiac hypertrophy, and aortic aneurysm exacerbation, we examined the morphological changes of the aortic valve at the time of preaneurysm (P7), aneurysm development (P14), and the expansion of an established aneurysm (P60; 2 months old). Coronal sections of the heart (including the aortic valve leaflets) were prepared from control, *ECKO*, *SMKO*, and *DKO* mice. Moreover, valve morphology was evaluated using hematoxylin and eosin and Masson trichrome staining. At P7, no differences in valve thickness were observed among genotypes (Figure 5A). However, at P14, *DKO* mice exhibited significantly thickened aortic valves (average 80.29 μm) compared with control (average 58.27 μm) and *ECKO* (average 56.01 μm) mice (Figure 5B). Because there was no difference in the heart weight to body weight ratio among genotypes at this time and no correlation was found between

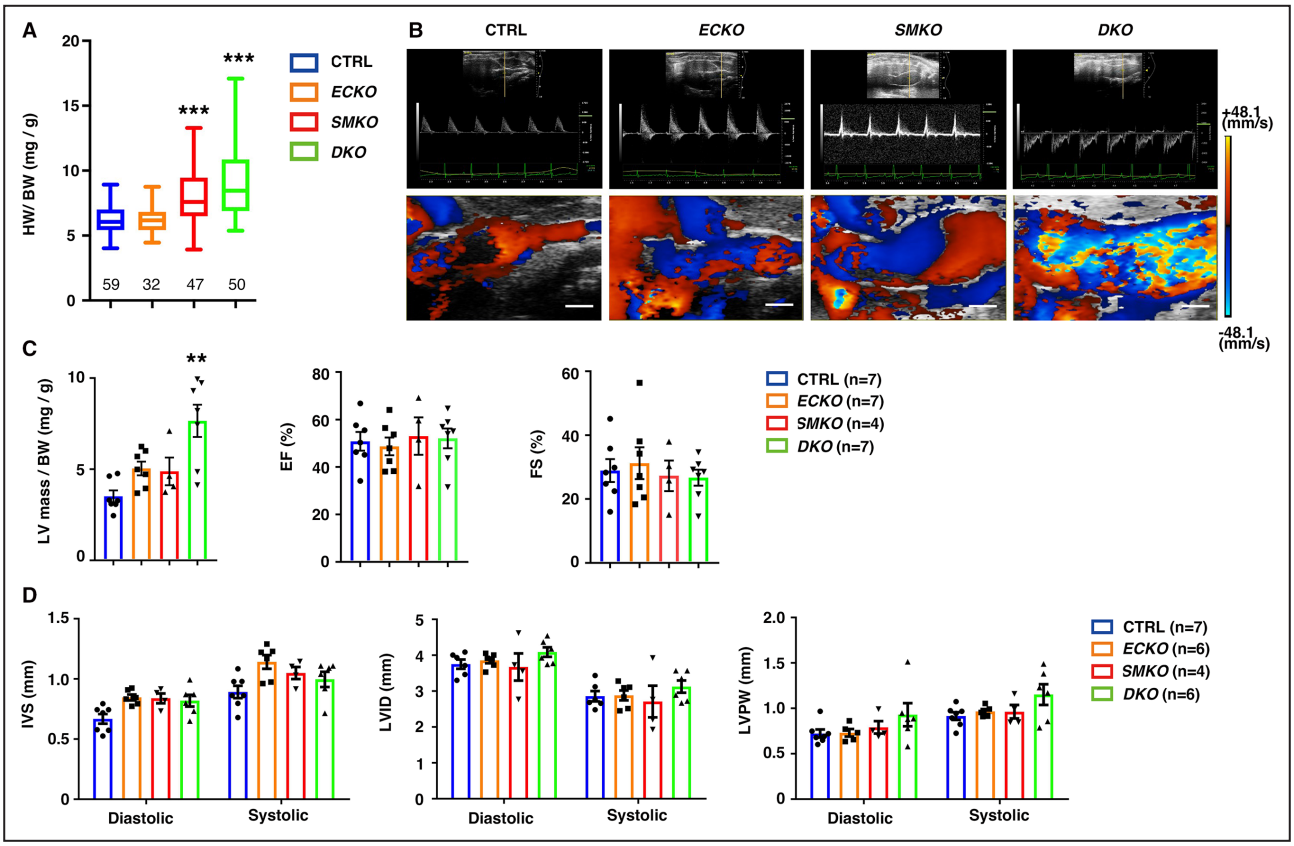

Figure 4. *DKO* mice showed cardiac hypertrophy and turbulent flow in the ascending aorta.
A, Cardiac hypertrophy was evaluated by measuring HW/BW. CTRL (n=59), *ECKO* (n=32), *SMKO* (n=47), and *DKO* (n=50) mice. Box plots show the median with interquartile range. Whiskers: minimum to maximum. ***P<0.001, Kruskal-Wallis test. **B**, (Upper panel) Representative images of transaortic flow velocity by pulse wave Doppler tracing of ascending aorta. Measurement points are indicated by yellow lines. Light green lines represent 1000 mm/s velocity and green curves indicate ECG. (Lower panel) Representative images of color Doppler in ascending aorta. Red, antegrade flow; blue, retrograde flow; yellow, turbulent flow. CTRL (n=9), *ECKO* (n=5), *SMKO* (n=9), and *DKO* (n=12). Scale bars are 1 mm. **C**, Quantification of LV mass to BW, EF, and FS. CTRL (n=7); *ECKO* (n=7); *SMKO* (n=4) and *DKO* (n=7). Bars are means ± SEM. **P<0.01, 1-way ANOVA. **D,** Quantification of the IVS, LVID, and LVPW in the cardiac cycle (diastolic and systolic). CTRL (n=7), *ECKO* (n=6), *SMKO* (n=4), and *DKO* (n=6) mice. Bars are means ± SEM, 1-way ANOVA. All mice were evaluated at 2 months old. BW indicates body weight; CTRL, control; *DKO*, double knockout; *ECKO*, endothelial cell–specific knockout; EF, ejection fraction; FS, fractional shortening; HW/BW, heart weight to body weight ratio; IVS, interventricular septum; LV, left ventricular; LVID, left ventricular internal dimension; LVPW, left ventricular posterior wall; and *SMKO*, smooth muscle cell–specific knockout.

heart weight to body weight ratio and valve thickness (Figure S7), valve abnormality was not a direct consequence of cardiac hypertrophy or vice versa. Thickened valve phenotype in *DKO* mice was more evident at P60 (Figure 5C), even if other heart valves, including pulmonary, mitral, and tricuspid valves did not show abnormal morphology (Figure S8). The excessive collagen deposition was only observed in the *DKO* mice at P60 (Figure 5C, yellow arrowheads). The excessive collagen production in the *DKO* aortic valve leaflets indicates progressive fibrosis in aortic valves after birth, which could be responsible for thickened aortic valves and associated turbulent flow in *DKO* mice. Because valve abnormality did not precede aneurysm formation at P7, we could not establish the causal relationship between valve abnormality and aneurysm progression. Nevertheless, turbulent flow caused by valve thickening had profound effects on the worsening of aortic aneurysms and cardiac hypertrophy.

Gene Expression Profile in the Aortic Valves of *DKO* Mice

To explore the molecular basis of aortic valve abnormality caused by *Fbln4* deficiency, we conducted RNA-seq using aortic valves from 2-month-old control, *ECKO*, *SMKO*, and *DKO* mice. Aortic valves were sectioned transversely, and samples were taken using laser-captured microdissection for RNA extraction (Figure 6A). As with the results of the aortic valve phenotype, principal component analysis, and hierarchical clustering on the heat map clearly separated *DKO* mice from the other groups (Figure S9). The Venn diagram shows 120 genes that were

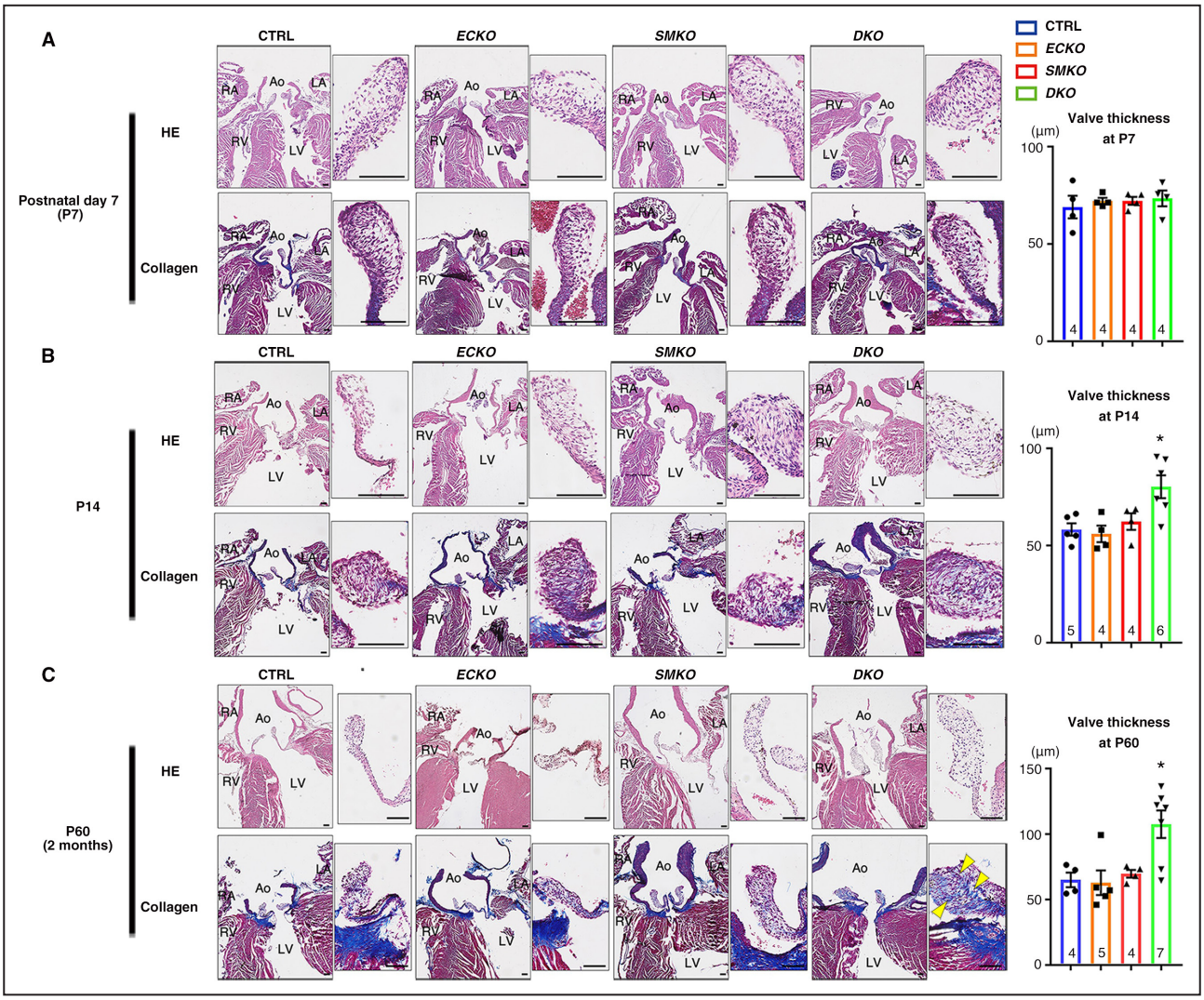

Figure 5. *DKO* mice showed aortic valve thickening accompanied by aneurysm formation.
A–C, Histological images of the aortic valve from CTRL, *ECKO*, *SMKO*, and *DKO* at P7 (in A), P14 (in B), and P60 (in C) stained with HE, and Masson trichrome (collagen). High magnification images are shown on the right. Yellow arrowheads show the accumulation of collagen in the *DKO* valve at P60. Scale bars are 100 μm. Quantification of aortic valve thickness is shown on the right. Animal numbers are indicated in the graph. Bars are means ± SEM. *P<0.05, 1-way ANOVA. Ao indicates aorta; CTRL, control; *DKO*, double knockout; *ECKO*, endothelial cell–specific knockout; HE, hematoxylin and eosin; LA, left atrium; LV, left ventricle; P, postnatal day; RA, right atrium; and RV, right ventricle.

differentially expressed (fold change greater than ±2, P<0.05) among the groups of *DKO* versus control, *DKO* versus *ECKO*, and *DKO* versus *SMKO* (Figure 6B). Gene ontology enrichment analysis of 120 genes allowed us to focus on the top 9 enriched biological processes including 36 genes involved in cyclic guanosine monophosphate–mediated signaling, the mitogen-activated protein kinase cascade, EC migration, and heart development (Figure 6C). A list of these 36 genes is shown in a heat map and volcano plots (Figure 6D). Additionally, a Circos plot presents the relationship between these genes and the existing group of genes known to be involved in valve fibrosis and calcification (Figure 6E). Gene set enrichment analysis revealed positive correlations between *DKO* and endothelial-to-mesenchymal transition (EndMT), inflammatory response, mTORC1 signaling, and the p53 pathway, whereas gene expression in *DKO* aortic valves had low correlations with Notch signaling and Wnt/β-catenin signaling (Figure 6F). Finally, we examined the changes in aortic valves and VICs by immunostaining. At P14, aortic valves of *DKO* mice expressed both α-smooth muscle actin (α-SMA) and CD31 and a significant increase in the number of α-SMA/CD31 double-positive cells were observed, suggesting the EndMT phenotype (Figure 7A). The

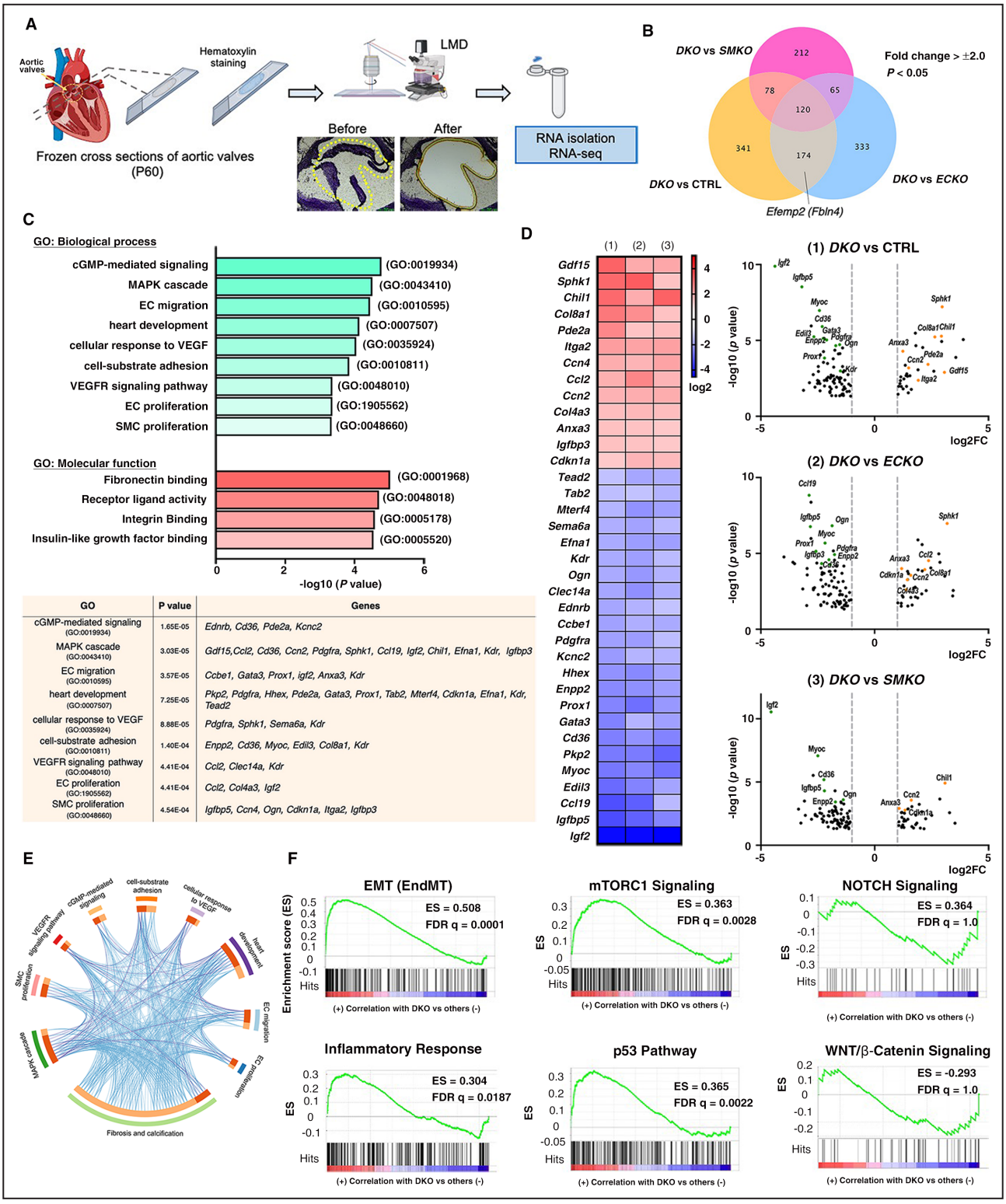

GO	P value	Genes
cGMP-mediated signaling (GO:0019934)	1.65E-05	*Ednrb, Cd36, Pde2a, Kcnc2*
MAPK cascade (GO:0043410)	3.03E-05	*Gdf15,Ccl2, Cd36, Ccn2, Pdgfra, Sphk1, Ccl19, Igf2, Chil1, Efna1, Kdr, Igfbp3*
EC migration (GO:0010595)	3.57E-05	*Ccbe1, Gata3, Prox1, igf2, Anxa3, Kdr*
heart development (GO:0007507)	7.25E-05	*Pkp2, Pdgfra, Hhex, Pde2a, Gata3, Prox1, Tab2, Mterf4, Cdkn1a, Efna1, Kdr, Tead2*
cellular response to VEGF (GO:0035924)	8.88E-05	*Pdgfra, Sphk1, Sema6a, Kdr*
cell-substrate adhesion (GO:0010811)	1.40E-04	*Enpp2, Cd36, Myoc, Edil3, Col8a1, Kdr*
VEGFR signaling pathway (GO:0048010)	4.41E-04	*Ccl2, Clec14a, Kdr*
EC proliferation (GO:1905562)	4.41E-04	*Ccl2, Col4a3, Igf2*
SMC proliferation (GO:0048660)	4.54E-04	*Igfbp5, Ccn4, Ogn, Cdkn1a, Itga2, Igfbp3*

expressions of α-SMA (also known as a marker for activated VICs[25]) and connective tissue growth factor (CTGF; involved in valvular fibrosis[26]) were significantly upregulated in *DKO* valves at 2 months old (Figure 7B and 7C). Additionally, growth differentiation factor-15 (Gdf15), which belongs to the TGF-β superfamily and has recently been shown to increase in cardiac fibrosis,[27] was increased in the *DKO* valves (Figure 7D). These results indicate that *Fbln4* deficiency in ECs may induce EndMT to generate activated VICs and cause valvular thickening and fibrosis, which subsequently promotes TAAs.

Figure 6. Gene expression profiles in aortic valves from *DKO* mice compared with CTRL, *ECKO*, and *SMKO* mice.
A, Aortic valves were obtained from CTRL (n=3), *ECKO* (n=3), *SMKO* (n=3), and *DKO* (n=3) mice at P60 by using a LMD system. **B**, Venn diagram summarizing the overlapping genes among indicated comparisons. *DKO* vs CTRL (yellow circle), *DKO* vs *ECKO* (light blue circle), and *DKO* vs *SMKO* (pink circle) mice. Fold change >±2, $P \leq 0.05$. *Efemp2* (*Fbln4*) belongs to the gray circle. **C**, Functional enrichment analysis of 120 genes, overlapped in the Venn diagram (in **B**). The negative $\log_{10}$ of the *P* value. The enriched GO terms associated with a biological process (light green) and molecular function (light red) are shown. Gene lists are shown at the bottom. **D**, Heat map of genes, listed in enrichment analysis (in C). Volcano plots of genes between the 2 conditions: (1) *DKO* vs CTRL, (2) *DKO* vs *ECKO*, and (3) *DKO* vs *SMKO* mice. The *P* value ($-\log_{10}$) was calculated and plotted against the $\log_2$ fold change (log2FC) for 120 genes. **E**, Circos plot and molecular interaction with picked up 36 genes and the fibrosis/calcification marker genes by Metascape. **F**, GSEA shows a correlation with biological pathways between *DKO* and other groups. A positive ES indicates gene set enrichment at the top of the ranked list. Gene sets were considered significantly enriched when the FDR *q* value was <0.05. CTRL indicates control; *DKO*, double knockout; *ECKO*, endothelial cell–specific knockout; EndMT, endothelial-to-mesenchymal transition; ES, enrichment score; Fbln4, fibulin-4; FDR, false discovery rate; GO, gene ontology; GSEA, gene set enrichment analysis; LMD, laser-captured microdissection; mTORC1, mechanistic/mammalian target of rapamycin complex 1; P, postnatal day; RNA-seq, RNA sequencing; and *SMKO*, smooth muscle cell–specific knockout.

DISCUSSION

In addition to SMCs, there is a growing appreciation of the importance of ECs, aortic valves, and cardiac hypertrophy in the formation of TAAs. Because mutations in *FBLN4* in humans are often neonatal lethal and cause severe vascular pathologies, including severe TAA,[28] early diagnosis and intervention are essential.[29–31] The *SMKO* mouse line serves as an excellent model to investigate the mechanism of vascular pathologies because the mutation does not cause rapid rupture or dissection and allows us to observe temporal changes in TAA initiation and progression.[13,15–17] In this study, we first reported that *FBLN4* deletion altered the morphology and transcriptome of ECs in vitro and that the genetic deletion of *Fbln4* in both ECs and SMCs (*DKO*) in vivo progressed TAA when compared with *SMKO*, thereby unraveling the protective function of EC-derived fibulin-4. Second, we observed aortic valve thickening with collagen deposition and the parallel progression of TAA starting at P14 in *DKO* mice, indicating that the loss of valvulo-arterial integrity was an exacerbating factor for TAA. Third, our RNA-seq analysis identified 36 genes involved in proliferation and tissue fibrosis that were significantly altered in *DKO* valves. Moreover, we confirmed increased protein levels of α-SMA, connective tissue growth factor, and Gdf15, which suggests the transdifferentiation (activation) of VICs and tissue fibrosis as an underlying cause of aortic valve thickening. Our study provides evidence of the pathological interactions of aortic valve abnormality and aortopathy resulting from the loss of fibulin-4 as progressive factors for TAA.

Synergistic Role of EC- and SMC-Derived Fibulin-4 in the Protection of TAAs

Fibulin-4 is a member of the fibulin family. It contains a section of calcium-binding epidermal growth factor–like tandem repeats and a C-terminal fibulin domain. Notably, it is known to play an important role in ECM assembly and elastogenesis.[32] Fibulin-4 tethers lysyl oxidase and fibulin-5 to monomeric elastin (tropoelastin) and interacts with latent TGF-β–binding protein-4L, thereby facilitating the crosslinking required for the nascent elastic fiber formation.[33,34] The deletion of *Fbln4* causes impaired elastogenesis, which results in defects in vascular formation that lead to perinatal lethality in mice.[35] Loss of *Fbln4* in SMCs causes a decreased ratio of filamentous actin (F-actin) to monomeric actin (G-actin), which alters the actin cytoskeleton and prevents SMC migration in vivo and in vitro.[16,36] Although these roles of fibulin-4 have been reported in vivo, the results are largely focused on SMCs and fibroblasts; however, their role in ECs has not yet been explored. Consistent with a previous finding,[13] we showed that loss of *Fbln4* only in ECs (*ECKO*) in mice does not produce gross abnormalities such as aortic aneurysms and defects in cardiac function. This result seemingly precluded the function of fibulin-4 in ECs. However, a recent study has shown that secreted extracellular fibulin-4 is taken up by mouse embryonic fibroblasts and recycled to activate lysyl oxidase.[37] Therefore, it is possible that fibulin-4 secreted from other vascular cells or circulating fibulin-4 is taken up by ECs and compensates for the fibulin-4 deficiency in the *ECKO* mice.

To investigate the mechanism of aneurysm enlargement in *DKO* mice, molecular signals were compared with those of *SMKO* mice. Our results showed that Thbs1 is upregulated in the ascending aortas of both *DKO* and *SMKO* mice and that this expression extended to the descending aorta in *DKO* mice. Thbs1 is highly expressed in the aneurysmal wall of TAA and abdominal aortic aneurysms[17,38] and is involved in shear stress–induced arterial stiffening and mechanotransduction in SMCs.[39,40] Thus, our results suggest that the entire *DKO* aorta was under intense mechanical stress when compared with *SMKO* aorta. The Src family of protein kinases is known to serve key roles in the regulation of signal transduction and the activation of many target molecules to regulate cellular functions.[41] Although precise target molecules were not identified in *DKO* aorta, Src is known to be a promising target for the treatment of cardiovascular diseases,[42] and further analysis is needed.

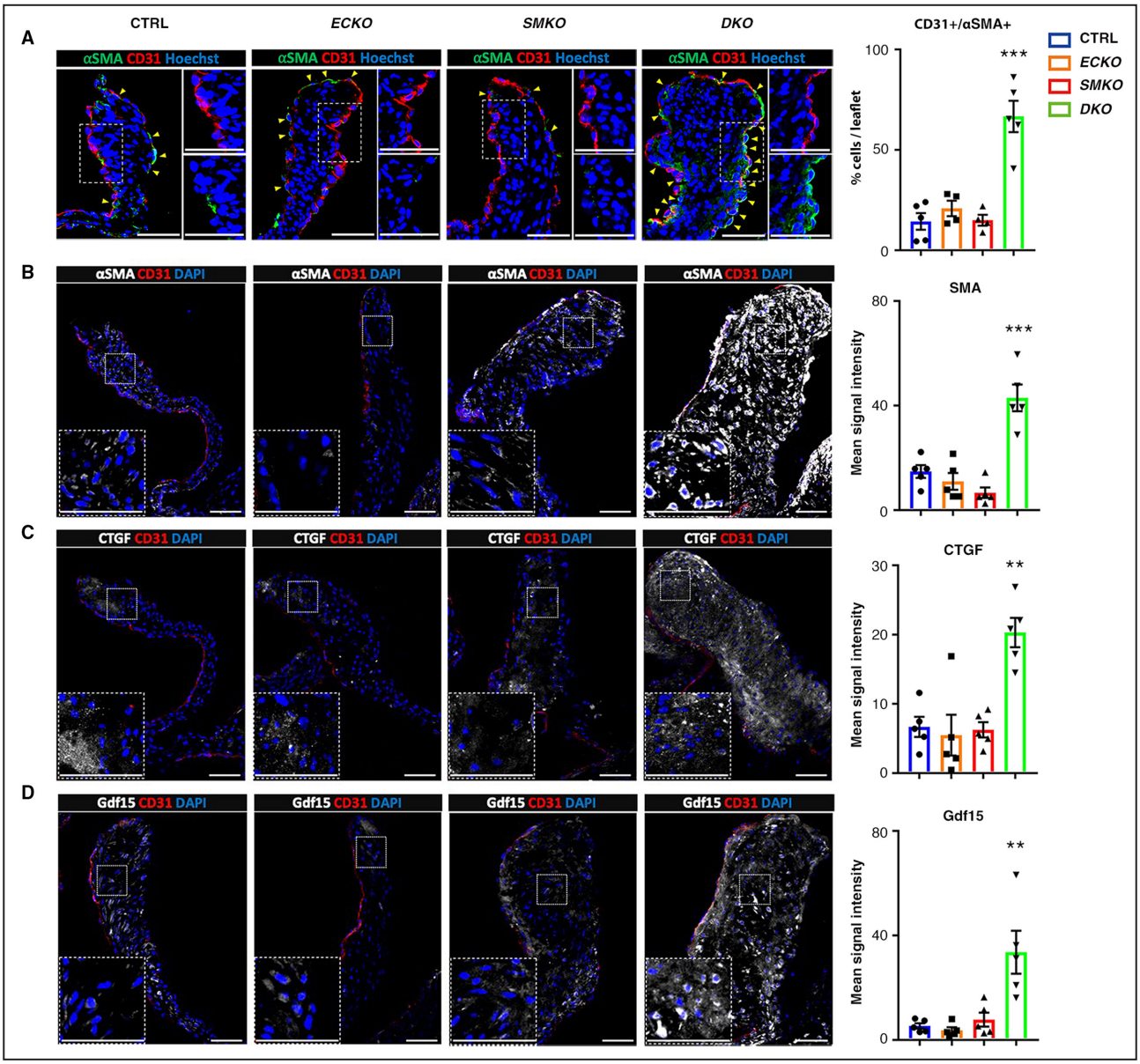

Figure 7. VICs are activated in the aortic valves of *DKO* mice.
A, Immunostaining with CD31 (known as an endothelial marker [red]), αSMA (green), and Hoechst (blue) in aortic valve leaflets from CTRL (n=5), *ECKO* (n=4), *SMKO* (n=4), and *DKO* (n=5) mice at postnatal day 14. High magnified images for single channel with Hoechst are shown on the right (white box). Percentage of CD31+ cells coexpressing αSMA per leaflet is shown on the right. Bars are means ± SEM. ***P<0.001, 1-way ANOVA. **B**–**D**, Immunostaining with CD31 (red) and αSMA (gray in **B**), CTGF (gray in **C**) and Gdf15 (gray in **D**) in aortic valve leaflets from CTRL (n=5), *ECKO* (n=5), *SMKO* (n=5), and *DKO* (n=5) mice at 2 months old. DAPI (blue) is shown and high magnified images are indicated in the white-dashed box. Quantification of mean signal intensity is shown on the right. Bars are means ± SEM. **P<0.01, ***P<0.001, 1-way ANOVA. αSMA indicates α-smooth muscle actin; CD31, cluster of differentiation 31; CTGF, connective tissue growth factor; CTRL, control; *DKO*, double knockout; *ECKO*, endothelial cell–specific knockout; Gdf15, growth differentiation factor-15; *SMKO*, smooth muscle cell–specific knockout; and VICs, valve interstitial cells.

The role of fibulin-4 in ECs and epithelial cells has recently been reported by several studies. Chen et al used single-cell RNA-seq to explore the molecular pathology of atherosclerosis by comparing the EC-specific knockout of TGF-β receptors on an *ApoE*$^{-/-}$ background, which were given either a high-fat or normal diet. Interestingly, *Fbln4* expression was increased in the high-fat feeding control group, whereas its expression decreased in EC-specific knockout of TGF-β receptors on an *ApoE*$^{-/-}$ background mice, and fibulin-4 was classified as a cluster of molecules involved in EndMT and the targets of TGF-β signaling and mesenchymal markers.[43] Zhou et al reported that *FBLN4* was highly expressed in patients with bladder cancer and that the deletion of *FBLN4* in human bladder cancer cells significantly reduced the epithelial

marker E-cadherin and increased mesenchymal markers, including N-cadherin, vimentin, and Snail and Slug, as well as the Wnt/β-catenin signaling pathway, thereby leading to epithelial-to-mesenchymal transition.[44] The overexpression of *FBLN4* in bladder cancer cells prevented bladder cancer growth and pulmonary metastasis in a mouse xenograft model. Additionally, Song et al reported that *FBLN4* expression was negatively correlated with malignancy in human lung cancer and that overexpression of *FBLN4* inhibited the invasion of lung cancer cells by decreasing the activity of matrix metalloproteinase-2 and metalloproteinase-9.[45] Our findings indicate that *FBLN4* deletion in HAECs-induced mesenchymal cell morphology and altered the gene expression profile related to EndMT are consistent with other studies of fibulin-4 in EndMT and warrant further analysis.

Possible Function of Fibulin-4 in Valvulo-Arterial Integrity

In this study, we observed thickening of aortic valves in *DKO* mice from P14 to P60 with collagen deposition, and these changes were specific to *DKO* mice. Apart from the well-known causal relationship between bicuspid aortic valve and the development of TAAs,[46] it remains unclear how aortic valve thickening affects the progression of aortic aneurysms or whether aortic aneurysms induce secondary valve abnormalities. Valve leaflets are mainly composed of two cell populations—an outside monolayer of ECs and VICs—which are derived primarily from endocardial ECs and ECM layers.[47,48] Several studies have identified neural crest–derived cells, such as melanocytes, dendric cells, and epicardium-derived cells, as an alternative source of valve progenitors.[49–51] Therefore, the fibulin-4 derived from these cells might compensate for the loss of endothelial *Fbln4* in the *ECKO* valve. It has been reported that increased ECM production, disorganization of the ECM, and the disarray of VICs can cause the thickening and dysfunction of aortic valves.[52] A single-cell RNA-seq analysis by Hulin et al has shown that the ECM genes such as collagens and glycosaminoglycans are highly variable in VICs, while gene expression in endothelial and immune cells was largely unchanged during heart valve maturation.[53] Our RNA-seq analysis of the aortic valve revealed that the mitogen-activated protein kinase cascade and a group of genes involved in EC proliferation, migration, and heart development are variably expressed in the *DKO* valves at 2 months. GDF15 was one of the genes downregulated in *FBLN4*-deficient HAECs but was highly expressed in the aortic valve of *DKO* mice. Because GDF15 is known to mediate antiaging and anti-inflammatory responses,[54,55] while also being involved in fibrosis, it is plausible that the compensatory upregulation of GDF15 in response to impaired valvulo-arterial integrity facilitated fibrotic changes in the *DKO* valves. Although Kim et al reported that epithelial-to-mesenchymal transition does not occur during adult valve homeostasis,[56] we could not exclude the possibility that *DKO* valves may be thickened via the EndMT processes. Mechanistically, it is difficult to decipher whether the loss of *Fbln4* induces gene expression in VICs and ECs by altering the ECM environment or directly acting on these cells through putative fibulin-4 cell surface receptors. A more detailed investigation is required for the molecular mechanism of the action of fibulin-4 in aortic valves and aortas.

CONCLUSIONS

We provided evidence that endothelial Fbln4 is essential for valvulo-arterial integrity by possibly suppressing EndMT in the aortic valves and maintaining the integrity of the aortic wall, both of which play a critical role in preventing the progression of aneurysm expansion. Because we observed aortic valve thickening, and aortic dilatation occurred at the same time during the neonatal period, we could not determine the precise cause-effect relationship between the two. Nevertheless, our study provides in vivo evidence for the pathological interactions of tricuspid aortic valve abnormality, including aortic stenosis and aortic insufficiency, and aortopathy synergistically exacerbates TAA. Therefore, we propose that routine monitoring and assessment of the aortic valve functions in patients with TAA is helpful for the prediction of clinical outcomes for TAA.

ARTICLE INFORMATION

Received May 26, 2022; accepted November 23, 2022.

Affiliations

Life Science Center for Survival Dynamics, Tsukuba Advanced Research Alliance (T.A.N., H.T.H., B.Q.T., S.J.S., K.S., Y.Y., H.Y.); and Ph.D. Program in Human Biology, School of Integrative and Global Majors (T.A.N.), University of Tsukuba, Ibaraki, Japan; Department of Anatomy, University of Sao Paulo, Institute of Biomedical Sciences, Sao Paulo, Brazil (C.A.L.); Graduate School of Comprehensive Human Sciences, University of Tsukuba, Ibaraki, Japan (H.T.H.); Department of Pharmacology, University of Sao Paulo, Ribeirao Preto Medical School, Ribeirao Preto, Brazil (J.V.A.); Deputy Head of Scientific Research Department- Training center, Cho Ray hospital, Ho Chi Minh City, Vietnam (B.Q.T.); Graduate School of Life and Environmental Sciences, University of Tsukuba, Ibaraki, Japan (S.J.S.); Institute for Advanced Research of Biosystem Dynamics, Waseda Research Institute for Science and Engineering, Waseda University, Tokyo, Japan (K.S., H.T.); Research organization for Nano and Life Innovation (H.M., H.T.); and Department of Life Science and Medical Bioscience (H.T.), Waseda University, Tokyo, Japan; Computational Bio Big-Data Open Innovation Laboratory, AIST-Waseda University, Tokyo, Japan (H.T.); Faculty of Medicine, University of Tsukuba, Ibaraki, Japan (H.Y.); and Now with Department of Advanced Medical Technologies, National Cerebral and Cardiovascular Center Research Institute, Osaka, 564-8565, Japan.

Acknowledgments

We thank M. Higashi (University of Tsukuba), K. Ranganathan (University of Tsukuba), and N. Suzuki (Waseda University) for their technical assistance, as

well as Y. Jinzenji for her assistance with electron microscopy (University of Tsukuba). We also thank J. Ishida (University of Tsukuba) for his assistance with Evans blue injection experiments. Figure 6A was created with BioRender.com.

Sources of Funding

This work was supported in part by the Japan Foundation for Applied Enzymology and Takeda Science Foundation, the MSD Life Science Foundation, KANAE Foundation for the Promotion of Medical Science, the NOVARTIS Foundation for the Promotion of Science, the MITSUBISHI Foundation, Japan Intractable Diseases (Nanbyo) Research Foundation (all to Y.Y.), as well as the Japan Society for the Promotion of Science (JSPS) KAKENHI (grant number JP21H02677 to Y.Y. and JP20H03762 to H.Y.) and the Japan Agency for Medical Research and Development (AMED) (grant number JP21ek0210158 to Y.Y. and JP21ek0109553h001 to H.Y.). This research was also supported by the Platform Project for Supporting Drug Discovery and Life Science Research (Basis for Supporting Innovative Drug Discovery and Life Science Research [BINDS]) from AMED under Grant Number JP21am0101104. The supercomputing resource was provided by the Human Genome Center (the University of Tokyo). T.A.V. Nguyen was supported by the Human Biology Program Fellowship of the University of Tsukuba and is a recipient of the Tokio Marine Kagami Memorial Foundation Scholarship. H.T. Hang was supported by the Japan Material International Scholarship Foundation. C.A. Lino was supported in part by the Ministry of Education, Culture, Sports, Science and Technology (MEXT) Inter-University Exchange Project. S.J. Shin was a recipient of the Honjo International Fellowship.

Disclosures

None.

Supplemental Material

Tables S1–S3
Figures S1–S9

REFERENCES

1. Pinard A, Jones GT, Milewicz DM. Genetics of thoracic and abdominal aortic diseases. *Circ Res*. 2019;124:588–606. doi: 10.1161/CIRCRESAHA.118.312436
2. Fletcher AJ, Syed MBJ, Aitman TJ, Newby DE, Walker NL. Inherited thoracic aortic disease: new insights and translational targets. *Circulation*. 2020;141:1570–1587.
3. Loeys BL, Chen J, Neptune ER, Judge DP, Podowski M, Holm T, Meyers J, Leitch CC, Katsanis N, Sharifi N, et al. A syndrome of altered cardiovascular, craniofacial, neurocognitive and skeletal development caused by mutations in TGFBR1 or TGFBR2. *Nat Genet*. 2005;37:275–281. doi: 10.1038/ng1511
4. Neptune ER, Frischmeyer PA, Arking DE, Myers L, Bunton TE, Gayraud B, Ramirez F, Sakai LY, Dietz HC. Dysregulation of TGF-beta activation contributes to pathogenesis in Marfan syndrome. *Nat Genet*. 2003;33:407–411. doi: 10.1038/ng1116
5. Milewicz DM, Prakash SK, Ramirez F. Therapeutics targeting drivers of thoracic aortic aneurysms and acute aortic dissections: insights from predisposing genes and mouse models. *Annu Rev Med*. 2017;68:51–67. doi: 10.1146/annurev-med-100415-022956
6. Yamashiro Y, Yanagisawa H. Crossing bridges between extra- and intra-cellular events in thoracic aortic aneurysms. *J Atheroscler Thromb*. 2018;25:99–110. doi: 10.5551/jat.RV17015
7. Lacro RV, Dietz HC, Sleeper LA, Yetman AT, Bradley TJ, Colan SD, Pearson GD, Selamet Tierney ES, Levine JC, Atz AM, et al. Atenolol versus losartan in children and young adults with Marfan's syndrome. *N Engl J Med*. 2014;371:2061–2071. doi: 10.1056/NEJMoa1404731
8. Hofmann Bowman MA, Eagle KA, Milewicz DM. Update on clinical trials of losartan with and without beta-blockers to block aneurysm growth in patients with Marfan syndrome: a review. *JAMA Cardiol*. 2019;4:702–707. doi: 10.1001/jamacardio.2019.1176
9. Galatioto J, Caescu CI, Hansen J, Cook JR, Miramontes I, Iyengar R, Ramirez F. Cell type-specific contributions of the angiotensin II type 1a receptor to aorta homeostasis and aneurysmal disease-brief report. *Arterioscler Thromb Vasc Biol*. 2018;38:588–591. doi: 10.1161/ATVBAHA.117.310609
10. Shen M, Hu M, Fedak PW, Oudit GY, Kassiri Z. Cell-specific functions of ADAM17 regulate the progression of thoracic aortic aneurysm. *Circ Res*. 2018;123:372–388. doi: 10.1161/CIRCRESAHA.118.313181
11. Gould RA, Aziz H, Woods CE, Seman-Senderos MA, Sparks E, Preuss C, Wunnemann F, Bedja D, Moats CR, McClymont SA, et al. ROBO4 variants predispose individuals to bicuspid aortic valve and thoracic aortic aneurysm. *Nat Genet*. 2019;51:42–50. doi: 10.1038/s41588-018-0265-y
12. Verma S, Siu SC. Aortic dilatation in patients with bicuspid aortic valve. *N Engl J Med*. 2014;370:1920–1929. doi: 10.1056/NEJMra1207059
13. Huang J, Davis EC, Chapman SL, Budatha M, Marmorstein LY, Word RA, Yanagisawa H. Fibulin-4 deficiency results in ascending aortic aneurysms: a potential link between abnormal smooth muscle cell phenotype and aneurysm progression. *Circ Res*. 2010;106:583–592. doi: 10.1161/CIRCRESAHA.109.207852
14. Halabi CM, Broekelmann TJ, Lin M, Lee VS, Chu ML, Mecham RP. Fibulin-4 is essential for maintaining arterial wall integrity in conduit but not muscular arteries. *Sci Adv*. 2017;3:e1602532. doi: 10.1126/sciadv.1602532
15. Huang J, Yamashiro Y, Papke CL, Ikeda Y, Lin Y, Patel M, Inagami T, Le VP, Wagenseil JE, Yanagisawa H. Angiotensin-converting enzyme-induced activation of local angiotensin signaling is required for ascending aortic aneurysms in fibulin-4-deficient mice. *Sci Transl Med* 2013;5:183ra158, 181–111.
16. Yamashiro Y, Papke CL, Kim J, Ringuette LJ, Zhang QJ, Liu ZP, Mirzaei H, Wagenseil JE, Davis EC, Yanagisawa H. Abnormal mechanosensing and cofilin activation promote the progression of ascending aortic aneurysms in mice. *Sci Signal.* 2015;8:ra105.
17. Yamashiro Y, Thang BQ, Shin SJ, Lino CA, Nakamura T, Kim J, Sugiyama K, Tokunaga C, Sakamoto H, Osaka M, et al. Role of thrombospondin-1 in Mechanotransduction and development of thoracic aortic aneurysm in mouse and humans. *Circ Res*. 2018;123:660–672. doi: 10.1161/CIRCRESAHA.118.313105
18. Shin SJ, Hang HT, Thang BQ, Shimoda T, Sakamoto H, Osaka M, Hiramatsu Y, Yamashiro Y, Yanagisawa H. Role of PAR1-Egr1 in the initiation of thoracic aortic aneurysm in Fbln4-deficient mice. *Arterioscler Thromb Vasc Biol*. 2020;40:1905–1917. doi: 10.1161/ATVBAHA.120.314560
19. Marshall LM, Carlson EJ, O'Malley J, Snyder CK, Charbonneau NL, Hayflick SJ, Coselli JS, Lemaire SA, Sakai LY. Thoracic aortic aneurysm frequency and dissection are associated with fibrillin-1 fragment concentrations in circulation. *Circ Res*. 2013;113:1159–1168. doi: 10.1161/CIRCRESAHA.113.301498
20. Oller J, Mendez-Barbero N, Ruiz EJ, Villahoz S, Renard M, Canelas LI, Briones AM, Alberca R, Lozano-Vidal N, Hurlé MA, et al. Nitric oxide mediates aortic disease in mice deficient in the metalloprotease Adamts1 and in a mouse model of Marfan syndrome. *Nat Med*. 2017;23:200–212. doi: 10.1038/nm.4266
21. Ren P, Zhang L, Xu G, Palmero LC, Albini PT, Coselli JS, Shen YH, LeMaire SA. ADAMTS-1 and ADAMTS-4 levels are elevated in thoracic aortic aneurysms and dissections. *Ann Thorac Surg*. 2013;95:570–577.
22. Yamashiro Y, Yanagisawa H. The molecular mechanism of mechanotransduction in vascular homeostasis and disease. *Clin Sci (Lond)*. 2020;134:2399–2418. doi: 10.1042/CS20190488
23. Maksuti E, Westerhof BE, Ugander M, Donker DW, Carlsson M, Broome M. Cardiac remodeling in aortic and mitral valve disease: a simulation study with clinical validation. *J Appl Physiol*. 1985;2019(126):1377–1389. doi: 10.1152/japplphysiol.00791.2018
24. Hanada K, Vermeij M, Garinis GA, de Waard MC, Kunen MG, Myers L, Maas A, Duncker DJ, Meijers C, Dietz HC, et al. Perturbations of vascular homeostasis and aortic valve abnormalities in fibulin-4 deficient mice. *Circ Res*. 2007;100:738–746. doi: 10.1161/01.RES.0000260181.19449.95
25. Walker GA, Masters KS, Shah DN, Anseth KS, Leinwand LA. Valvular myofibroblast activation by transforming growth factor-beta: implications for pathological extracellular matrix remodeling in heart valve disease. *Circ Res.* 2004;95:253–260. doi: 10.1161/01.RES.0000136520.07995.aa
26. Buttner P, Feistner L, Lurz P, Thiele H, Hutcheson JD, Schlotter F. Dissecting calcific aortic valve disease-the role, etiology, and drivers of valvular fibrosis. *Front Cardiovasc Med*. 2021;8:660797. doi: 10.3389/fcvm.2021.660797
27. Guo H, Zhao X, Li H, Liu K, Jiang H, Zeng X, Chang J, Ma C, Fu Z, Lv X, et al. GDF15 promotes cardiac fibrosis and proliferation of cardiac fibroblasts via the MAPK/ERK1/2 pathway after irradiation in rats. *Radiat Res*. 2021;196:183–191. doi: 10.1667/RADE-20-00206.1
28. Hucthagowder V, Sausgruber N, Kim KH, Angle B, Marmorstein LY, Urban Z. Fibulin-4: a novel gene for an autosomal recessive cutis laxa syndrome. *Am J Hum Genet*. 2006;78:1075–1080. doi: 10.1086/504304

29. Dasouki M, Markova D, Garola R, Sasaki T, Charbonneau NL, Sakai LY, Chu ML. Compound heterozygous mutations in fibulin-4 causing neonatal lethal pulmonary artery occlusion, aortic aneurysm, arachnodactyly, and mild cutis laxa. *Am J Med Genet A*. 2007;143A:2635–2641.
30. Hoyer J, Kraus C, Hammersen G, Geppert JP, Rauch A. Lethal cutis laxa with contractural arachnodactyly, overgrowth and soft tissue bleeding due to a novel homozygous fibulin-4 gene mutation. *Clin Genet*. 2009;76:276–281. doi: 10.1111/j.1399-0004.2009.01204.x
31. Thomas P, Venugopalan A, Narayanan S, Mathew T, Cherukuwada LPD, Chandran S, Pradeep J, Fitzgibbons TP, George V. Case report: occurrence of severe thoracic aortic aneurysms (involving the ascending, arch, and descending segments) as a result of fibulin-4 deficiency: a rare pathology with successful management. *Front Cardiovasc Med*. 2021;8:756765. doi: 10.3389/fcvm.2021.756765
32. Papke CL, Yanagisawa H. Fibulin-4 and fibulin-5 in elastogenesis and beyond: Insights from mouse and human studies. *Matrix Biol*. 2014;37:142–149. doi: 10.1016/j.matbio.2014.02.004
33. Horiguchi M, Inoue T, Ohbayashi T, Hirai M, Noda K, Marmorstein LY, Yabe D, Takagi K, Akama TO, Kita T, et al. Fibulin-4 conducts proper elastogenesis via interaction with cross-linking enzyme lysyl oxidase. *Proc Natl Acad Sci USA*. 2009;106:19029–19034. doi: 10.1073/pnas.0908268106
34. Kumra H, Nelea V, Hakami H, Pagliuzza A, Djokic J, Xu J, Yanagisawa H, Reinhardt DP. Fibulin-4 exerts a dual role in LTBP-4L-mediated matrix assembly and function. *Proc Natl Acad Sci USA*. 2019;116:20428–20437. doi: 10.1073/pnas.1901048116
35. McLaughlin PJ, Chen Q, Horiguchi M, Starcher BC, Stanton JB, Broekelmann TJ, Marmorstein AD, McKay B, Mecham R, Nakamura T, et al. Targeted disruption of fibulin-4 abolishes elastogenesis and causes perinatal lethality in mice. *Mol Cell Biol*. 2006;26:1700–1709. doi: 10.1128/MCB.26.5.1700-1709.2006
36. Burger J, van Vliet N, van Heijningen P, Kumra H, Kremers GJ, Alves M, van Cappellen G, Yanagisawa H, Reinhardt DP, Kanaar R, et al. Fibulin-4 deficiency differentially affects cytoskeleton structure and dynamics as well as TGFbeta signaling. *Cell Signal*. 2019;58:65–78. doi: 10.1016/j.cellsig.2019.02.008
37. Noda K, Kitagawa K, Miki T, Horiguchi M, Akama TO, Taniguchi T, Taniguchi H, Takahashi K, Ogra Y, Mecham RP, et al. A matricellular protein fibulin-4 is essential for the activation of lysyl oxidase. *Sci Adv*. 2020;6:eabc1404. doi: 10.1126/sciadv.abc1404
38. Liu Z, Morgan S, Ren J, Wang Q, Annis DS, Mosher DF, Zhang J, Sorenson CM, Sheibani N, Liu B. Thrombospondin-1 (TSP1) contributes to the development of vascular inflammation by regulating monocytic cell motility in mouse models of abdominal aortic aneurysm. *Circ Res*. 2015;117:129–141. doi: 10.1161/CIRCRESAHA.117.305262
39. Yamashiro Y, Thang BQ, Ramirez K, Shin SJ, Kohata T, Ohata S, Nguyen TA, Ohtsuki S, Nagayama K, Yanagisawa H. Matrix mechanotransduction mediated by thrombospondin-1/integrin/YAP in the vascular remodeling. *Proc Natl Acad Sci USA*. 2020;117:9896–9905. doi: 10.1073/pnas.1919702117
40. Kim CW, Pokutta-Paskaleva A, Kumar S, Timmins LH, Morris AD, Kang DW, Dalal S, Chadid T, Kuo KM, Raykin J, et al. Disturbed flow promotes arterial stiffening through Thrombospondin-1. *Circulation*. 2017;136:1217–1232. doi: 10.1161/CIRCULATIONAHA.116.026361
41. Parsons SJ, Parsons JT. Src family kinases, key regulators of signal transduction. *Oncogene*. 2004;23:7906–7909. doi: 10.1038/sj.onc.1208160
42. Zhai Y, Yang J, Zhang J, Yang J, Li Q, Zheng T. Src-family protein tyrosine kinases: a promising target for treating cardiovascular diseases. *Int J Med Sci*. 2021;18:1216–1224. doi: 10.7150/ijms.49241
43. Chen PY, Qin L, Li G, Wang Z, Dahlman JE, Malagon-Lopez J, Gujja S, Cilfone NA, Kauffman KJ, Sun L, et al. Endothelial TGF-beta signalling drives vascular inflammation and atherosclerosis. *Nat Metab*. 2019;1:912–926. doi: 10.1038/s42255-019-0102-3
44. Zhou Q, Chen S, Lu M, Luo Y, Wang G, Xiao Y, Ju L, Wang X. EFEMP2 suppresses epithelial-mesenchymal transition via Wnt/beta-catenin signaling pathway in human bladder cancer. *Int J Biol Sci*. 2019;15:2139–2155. doi: 10.7150/ijbs.35541
45. Song L, Li XX, Liu XY, Wang Z, Yu Y, Shi M, Jiang B, He XP. EFEMP2 suppresses the invasion of lung cancer cells by inhibiting epithelial-mesenchymal transition (EMT) and Down-regulating MMPs. *Onco Targets Ther*. 2020;13:1375–1396. doi: 10.2147/OTT.S236111
46. van de Pol V, Kurakula K, DeRuiter MC, Goumans MJ. Thoracic aortic aneurysm development in patients with bicuspid aortic valve: What is the role of endothelial cells? *Front Physiol*. 2017;8:938. doi: 10.3389/fphys.2017.00938
47. de Lange FJ, Moorman AF, Anderson RH, Manner J, Soufan AT, de Gier-de Vries C, Schneider MD, Webb S, van den Hoff MJ, Christoffels VM. Lineage and morphogenetic analysis of the cardiac valves. *Circ Res* 2004;95:645–654, DOI: 10.1161/01.RES.0000141429.13560.cb.
48. Combs MD, Yutzey KE. Heart valve development: regulatory networks in development and disease. *Circ Res*. 2009;105:408–421. doi: 10.1161/CIRCRESAHA.109.201566
49. Nakamura T, Colbert MC, Robbins J. Neural crest cells retain multipotential characteristics in the developing valves and label the cardiac conduction system. *Circ Res*. 2006;98:1547–1554. doi: 10.1161/01.RES.0000227505.19472.69
50. Choi JH, Do Y, Cheong C, Koh H, Boscardin SB, Oh YS, Bozzacco L, Trumpfheller C, Park CG, Steinman RM. Identification of antigen-presenting dendritic cells in mouse aorta and cardiac valves. *J Exp Med*. 2009;206:497–505. doi: 10.1084/jem.20082129
51. Wu B, Wang Y, Xiao F, Butcher JT, Yutzey KE, Zhou B. Developmental mechanisms of aortic valve malformation and disease. *Annu Rev Physiol*. 2017;79:21–41. doi: 10.1146/annurev-physiol-022516-034001
52. Hinton RB Jr, Lincoln J, Deutsch GH, Osinska H, Manning PB, Benson DW, Yutzey KE. Extracellular matrix remodeling and organization in developing and diseased aortic valves. *Circ Res*. 2006;98:1431–1438. doi: 10.1161/01.RES.0000224114.65109.4e
53. Hulin A, Hortells L, Gomez-Stallons MV, O'Donnell A, Chetal K, Adam M, Lancellotti P, Oury C, Potter SS, Salomonis N, et al. Maturation of heart valve cell populations during postnatal remodeling. *Development*. 2019;146:dev173047.
54. Moon JS, Goeminne LJE, Kim JT, Tian JW, Kim SH, Nga HT, Kang SG, Kang BE, Byun JS, Lee YS, et al. Growth differentiation factor 15 protects against the aging-mediated systemic inflammatory response in humans and mice. *Aging Cell*. 2020;19:e13195. doi: 10.1111/acel.13195
55. Carreras-Badosa G, Gomez-Vilarrubla A, Mas-Pares B, Xargay-Torrent S, Prats-Puig A, Puerto-Carranza E, de Zegher F, Ibanez L, Bassols J, Lopez-Bermejo A. Longitudinal association of the anti-inflammatory serum marker GDF-15 with serum IgA and IgG in apparently healthy children. *Sci Rep*. 2021;11:18215. doi: 10.1038/s41598-021-97386-1
56. Kim AJ, Alfieri CM, Yutzey KE. Endothelial cell lineage analysis does not provide evidence for EMT in adult valve homeostasis and disease. *Anat Rec (Hoboken)*. 2019;302:125–135. doi: 10.1002/ar.23916
57. Yamazaki M, Hosokawa M, Arikawa K, Takahashi K, Sakanashi C, Yoda T, Matsunaga H, Takeyama H. Effective microtissue RNA extraction coupled with smart-seq2 for reproducible and robust spatial transcriptome analysis. *Sci Rep*. 2020;10:7083. doi: 10.1038/s41598-020-63495-6

SUPPLEMENTAL MATERIAL

Data S1. Supplemental Material & Methods

All data supporting the findings of this study are available from the corresponding authors upon reasonable request.

Histology and morphometric analysis. Mouse aortas, hearts, and heart valves were harvested and perfusion-fixed with 4% paraformaldehyde and embedded in paraffin or embedded in Optimal Cutting Temperature (OCT) compound (SAKURA Finetek USA Inc., #4583). Paraffin sections of hearts (6 µm), aortic valves (8 µm), and aortas (5 µm) or frozen sections of pulmonary valves, mitral valves and tricuspid valves (10 µm) were stained with hematoxylin and eosin (HE), Hart's (elastic fibers), or Masson's trichrome (collagens). Images were digitally captured with SteREO Discovery V12 (ZEISS) and Axio Imager Z2 (ZEISS). Morphometric analysis was performed with Image J software (https://imagej.nih.gov/ij/index.html) as previously described[16,17]. Morphology of the heart cross sections were evaluated with a depth of more than 100 µm in the middle part of the heart. For heart valves, the hearts were sectioned coronally starting from the ventral to dorsal direction and valve leaflets with a depth of more than 150 µm were used to measure the valve thickness. Measured values were the average of three independent measurements per leaflet, and a total of 8 to 10 different sections per sample were counted.

Total aneurysmal surface analysis. Thoracic aortas were harvested, and adipose tissues were carefully removed. Aorta was open longitudinally from the aortic root to the left subclavian artery and captured images by SteREO Discovery V12 (ZEISS). The aneurysmal surface areas from the aortic root to the aortic arch were measured by Image J software.

Echocardiographic analysis. Echocardiography (Echo) was performed on 2-month-old mice using a Vevo 2100 imaging system (FUJIFILM VisualSonics Inc.). Mice were anesthetized with 2% isoflurane (flow approximately 1.5–2.0 L/min) and kept on a warmed platform to maintain optimal physiological conditions during Echo. M-mode was used to measure the aortic diameter and cardiac functions, including the ejection fraction (EF), fractional shortening (FS), interventricular septum (IVS), left ventricular posterior wall (LVPW), and left ventricular internal dimension (LVID). Color and pulse wave doppler modes were used for blood flow quantification.

Collection of aortic valves by laser-captured microdissection (LMD)

Hearts and aortic valves were harvested from CTRL (n=3), *ECKO* (n=3), *SMKO* (n=3), and *DKO* (n=3) mice after perfusion with 5 ml of 1xPBS. The tissues were immediately fixed with 4% paraformaldehyde, then washed with 20% sucrose and embedded in Optimal Cutting Temperature (OCT) compound (SAKURA Finetek USA Inc., #4583) to make frozen tissue samples. Cross-sections of the aortic valves (20 µm thickness) were mounted onto PEN-Membrane slides (Leica, #11600288) and stored at -80ºC until the LMD process. The aortic valve sections on the slide were replaced at room

temperature (RT) and dried using a hand circulator. The sections were fixed briefly with 100% ethanol and stained with hematoxylin solution (Muto Pure Chemicals Co., LTD, #30141) for 3 min, then incubated in a water bath at 30ºC for 15 min. Thereafter, the sections were cleaned with 100% ethanol and dried completely at RT. Whole aortic valve leaflets were captured using LMD7 (Leica) under the 10 x magnification and collected into MaxyClear (low adhesion) microtubes (Corning, PCR-02-L-C) with 20 µL of 99.5% ethanol and stored at -80ºC until cDNA library preparation.

RNA sequencing (RNA-seq) for aortic valve

The cDNA library was prepared from LMD-captured aortic valves using the Nextera XT DNA library prep kit (Illumina, FC-131-1024) as previously described[57]. The amplified 0.25 ng cDNA was used for RNA-seq library preparation and sequenced on a MiSeq (Illumina) with the paired-end 75-base read option. Reads (FASTQ files) were analyzed by using CLC Genomics Workbench (Version 22.0, QIAGEN). Trimmed sequences were mapped on the mouse genome (GRCm39.105). Differentially expressed genes were normalized by TMM (trimmed mean of M values) and analyzed using the Differential Expression tool in RNA-seq and small RNA analysis was performed on CLC Genomics Workbench.

Bioinformatics analysis

Gene Ontology analyses were performed using GO Consortium (http://www.geneontology.org). A Venn diagram was generated using the Create Venn Diagram for RNA-seq tool from CLC Genomics Workbench. A heat map and volcano plots were created using Prism 8 (Graph Pad, ver. 8.4.2). Log10 fold change of gene expression in si*FBLN4* compared to siSCR (in Fig. 1D), log2 fold change and *p*-value of gene expression in *DKO* compared to CTRL, *ECKO* or *SMKO* (in Fig. 6D) were generated by CLC Genomics Workbench. The -log10 (*p* value, in volcano plots in Fig. 6D) was generated by Excel. A Circos plot and transcriptional regulatory relationships unraveled by sentence-based text-mining (TRRUST) were conducted using Metascape (https://metascape.org). Gene set enrichment analysis (GSEA, https://www.gsea-msigdb.org/gsea/index.jsp) was used to generate false discovery rate (*q*-value) between the enrichment score of a gene set and the enrichment score of all gene sets against the dataset of biological pathway. Gene sets were considered significantly enriched with a biological pathway if the false discovery rate (FDR; *q*-value) was < 0.05.

Transmission electron microscopy. Aortas were dissected at 1–2 months old following cardiac perfusion with 3% glutaraldehyde in 0.1M sodium cacodylate solution (pH7.4), as previously described[3]. Ultra-thin sections were viewed and captured using a JEM1400 transmission electron microscopy (TEM, JEOL).

Permeability assay. Overall, 1 % of Evans blue (Sigma-Aldrich, E2129) was injected into 2- to 3-month-old mice via the lateral tail vein at a concentration of 10 ml/kg body weight. Aortas were

collected 1 h after the injection and perfused with saline from the left ventricle, harvested, and embedded into OCT compound for immunofluorescence staining. Images of aortas were digitally captured using SteREO Discovery V12 (ZEISS).

Table S1. Animals and breeding

Group	Breeding
CTRL ***ECKO*** ***SMKO*** ***DKO***	*Fbln4*$^{loxp/+}$; *SM22α-Cre*$^{+/-}$; *Tie2-Cre*$^{+/-}$ x *Fbln4*$^{KO/+}$; *SM22α-Cre*$^{+/-}$; *Tie2-Cre*$^{+/-}$

Mouse	Vendor or Source	Background Strain	Sex
Fbln4$^{loxp/+}$	Our laboratory (Huang et al. *Circ. Res.*, 2010)[13]	C57BL/6J;129SvEv	Both
Fbln4$^{KO/+}$	Our laboratory (Huang et al. *Circ. Res.*, 2010)[13]	C57BL/6J;129SvEv	Both
SM22α-Cre	The Jackson Laboratory (Stock#017491)	C57BL/6J;129SvEv	Both
Tie2-Cre	The Jackson Laboratory (Stock#008863)	C57BL/6J	Both

Group	Genotype
CTRL	*Fbln4*$^{loxp/+}$; *SM22α-Cre* (+) or (-); *Tie2-Cre* (+) or (-) *Fbln4*$^{+/+}$; *SM22α-Cre* (+) or (-); *Tie2-Cre* (+) or (-) *Cre* (+); *Cre*$^{+/-}$ *or* $^{+/+}$
ECKO	*Fbln4*$^{loxp/KO}$; *SM22α-Cre* (-); *Tie2-Cre* (+) *Cre* (+); *Cre*$^{+/-}$ *or* $^{+/+}$
SMKO	*Fbln4*$^{loxp/KO}$; *SM22α-Cre* (+); *Tie2-Cre* (-) *Cre* (+); *Cre*$^{+/-}$ *or* $^{+/+}$
DKO	*Fbln4*$^{loxp/KO}$; *SM22α-Cre* (+); *Tie2-Cre* (+) *Cre* (+); *Cre*$^{+/-}$ *or* $^{+/+}$

Table S2. Primer sequences for genotyping

Fbln4 KO	Forward 5'- CTTAGAGGGCCAGGGAGGTGAAGAC -3'
	Reverse 5'- CCCTGCCTCTACCTTTGCCCAAGAG -3'
Fbln4 flox (GTDL)	Forward 5'- CTGCCCCTTCAAGAAGCTGG -3'
(Cretest)	Reverse 5'- CCGGGATGGTCAGGCACTCG -3'
SM22α-Cre	Forward 5'- CGCATAACCAGTGAAACAGCATTGC -3'
	Reverse 5'- CAGACACCGAAGCTACTCTCCTTCC -3'
Tie2-Cre	Forward 5'- CGCATAACCAGTGAAACAGCATTGC -3'
	Reverse 5'- CCCTGTGCTCAGACAGAAATGAGA -3'

Table S3. Antibodies used for this study

Western blot analysis

Antibody	Dilution	Source	Catalog number
ACE	1:1000	Santa Cruz Biotechnology	sc-20791
Thbs1	1:500	Neomarkers	MS-421
Egr1	1:500	Cell Signaling	#4154
pSmad 2 (Ser465/467)	1:500	Cell Signaling	#3108
Smad2/3	1:1000	Cell Signaling	#8685
pERK (Thr202/Tyr204)	1:500	Cell Signaling	#4376
ERK1/2	1:1000	Cell Signaling	#9102
pSrc (Tyr416)	1:500	Cell Signaling	#6943
Src	1:1000	Cell Signaling	#2109
GAPDH	1:1000	Cell Signaling	#2118

ACE, angiotensin-converting enzyme; Thbs1, thrombospondin-1; Egr1, early growth response 1; p, phosphorylation; Smad, suppressor of mothers against decapentaplegic; ERK, extracellular signal-regulated kinase; Src, proto-oncogene tyrosine–protein kinase; GAPDH, glyceraldehyde 3-phosphate dehydrogenase.

Immunostaining

Antibody	Dilution	Source	Catalog number
CD31 (PECAM)	1:100 or 1:200	BD Biosciences	#550274
αSMA	1:200 or 1:300	Sigma-Aldrich	A5228
CTGF	1:200	Santa Cruz Biotechnology	sc-14939
Gdf15	1:100	Santa Cruz Biotechnology	sc-515675
Hoechst	1:1000	Sigma-Aldrich	B2261

CD31, cluster of differentiation 31; PECAM, platelet endothelial cell adhesion molecule 1; αSMA, α-smooth muscle actin; CTGF, connective tissue growth factor; Gdf15, growth differentiation factor-15.

Figure S1. Evaluation of aneurysm phenotype by echocardiography and transmission electron microscopy (TEM).

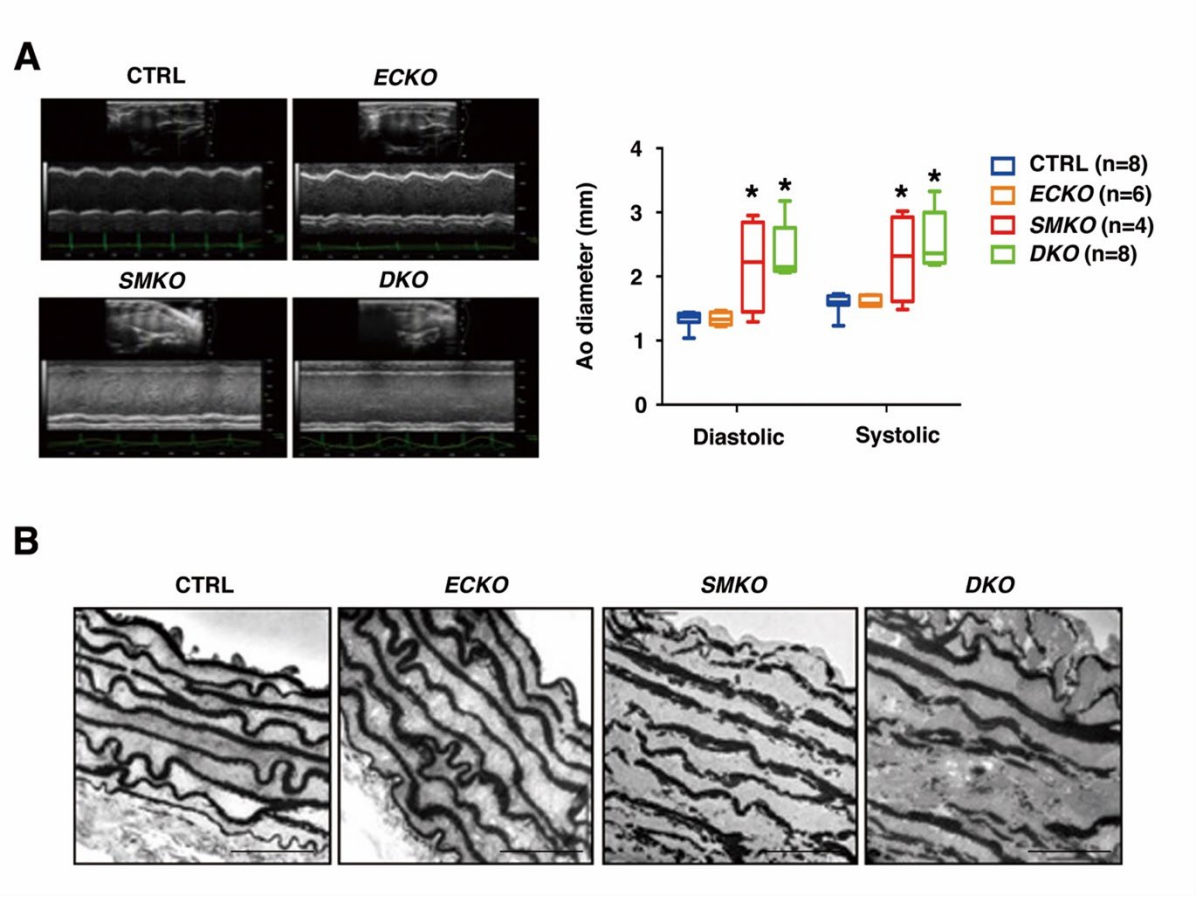

(**A**) Representative images and quantification of outer aortic (Ao) diameter during diastole and systole measured by echocardiography in control (CTRL, n=8), EC-specific knockout (ECKO, n=6), SMC-specific knockout (SMKO, n=4), and EC- and SMC- knockout (DKO, n=8). Box plots show the median with interquartile range. Whiskers: min to max. *$P < 0.05$, Kruskal-Wallis test. (**B**) TEM images of cross-sections of ascending aortas from 1–2 months old in CTRL (n=4), ECKO (n=3), SMKO (n=4), and DKO (n=2) mice. Scale bars are 10 µm.

Figure S2. Egr1 and Thbs1 are increased in the descending aorta of DKO mice.

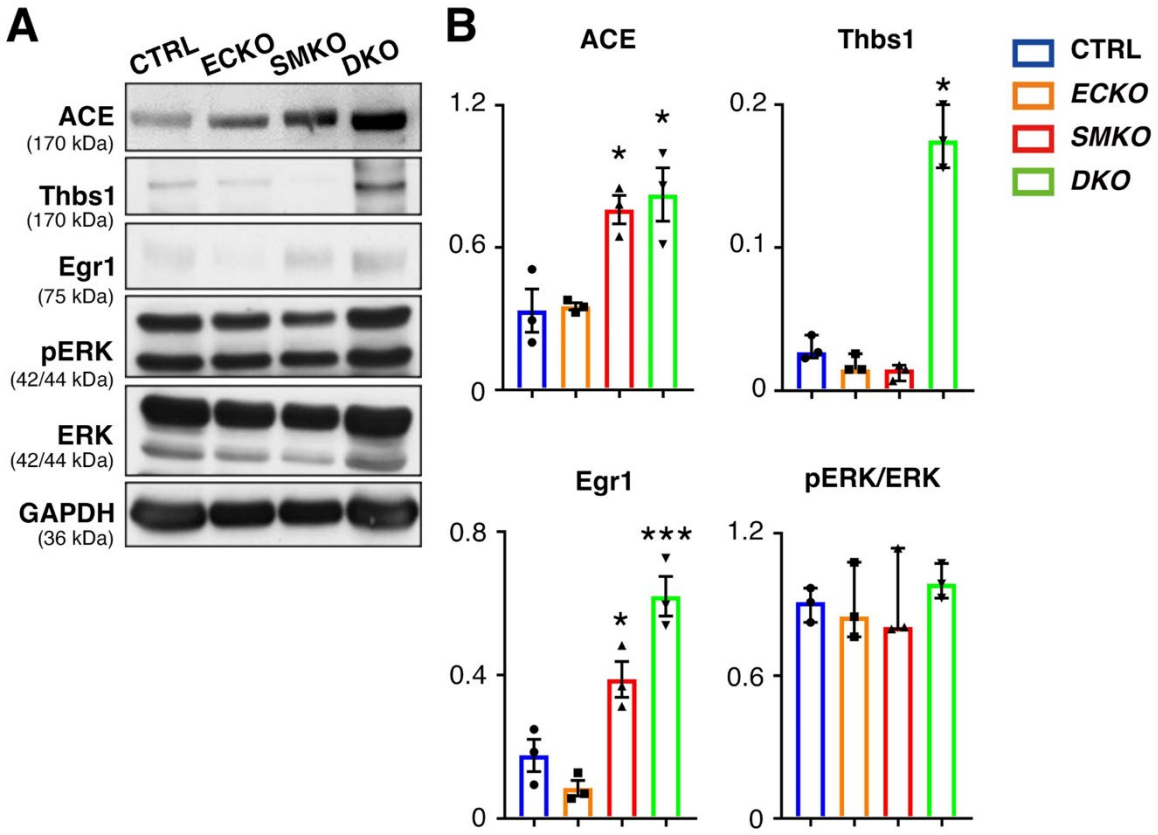

(**A**) Representative western blots of descending aortas from CTRL (n=3, pooled 3 aortas per group), ECKO (n=3, pooled 2 aortas per group), SMKO (n=3, 1 aorta per group), and DKO (n=3, pooled 2 aortas per group) mice. ACE, angiotensin-converting enzyme; Thbs1, thrombospondin-1; Egr1, early growth response 1; p, phosphorylation; ERK, extracellular signal-regulated kinase; GAPDH, glyceraldehyde 3-phosphate dehydrogenase. (**B**) Quantification graph of western blots is shown. *$P < 0.05$, ***$P < 0.001$, one-way ANOVA for ACE and Egr1, bars are means ± SEM. Kruskal-Wallis test for Thbs1 and pERK, bars are median with min to max range.

Figure S3. Evans blue (EB) injection to evaluate vascular permeability.

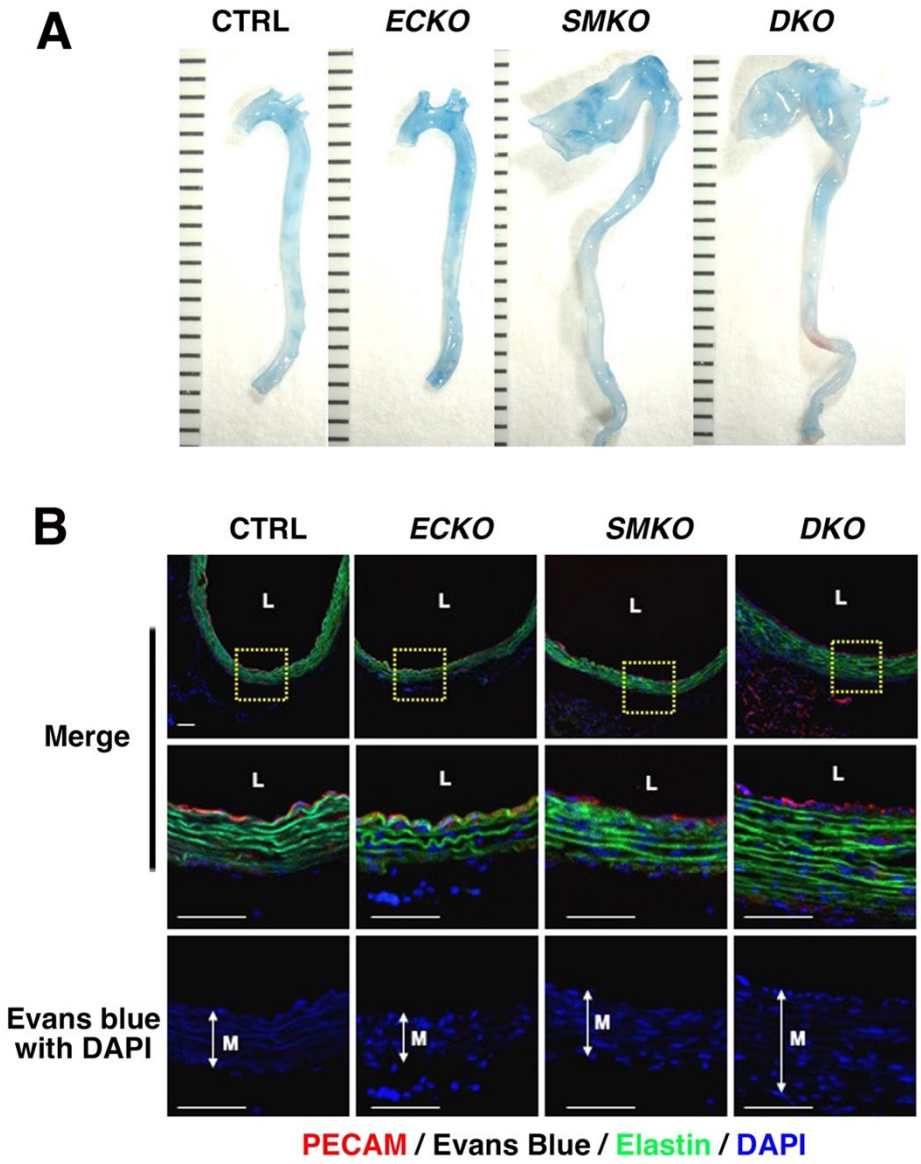

(**A**) 1% EB was injected via the lateral tail vein. 1 hour after injection, vascular permeability was evaluated for EB leakage to the aortic wall. Representative gross images of EB-injected aortas from CTRL, ECKO, SMKO, and DKO mice (n=3 per genotype). Scale bars are 1 cm. (**B**) Immunostaining with PECAM (as an endothelial cell marker, red), 647-conjugated Evans blue (white), autofluorescence of elastin (green), and DAPI (blue) are shown. L, lumen; M, medial layer. Scale bars are 50μm. PECAM, platelet endothelial cell adhesion molecule 1.

Figure S4. Morphological analysis of left ventricles.

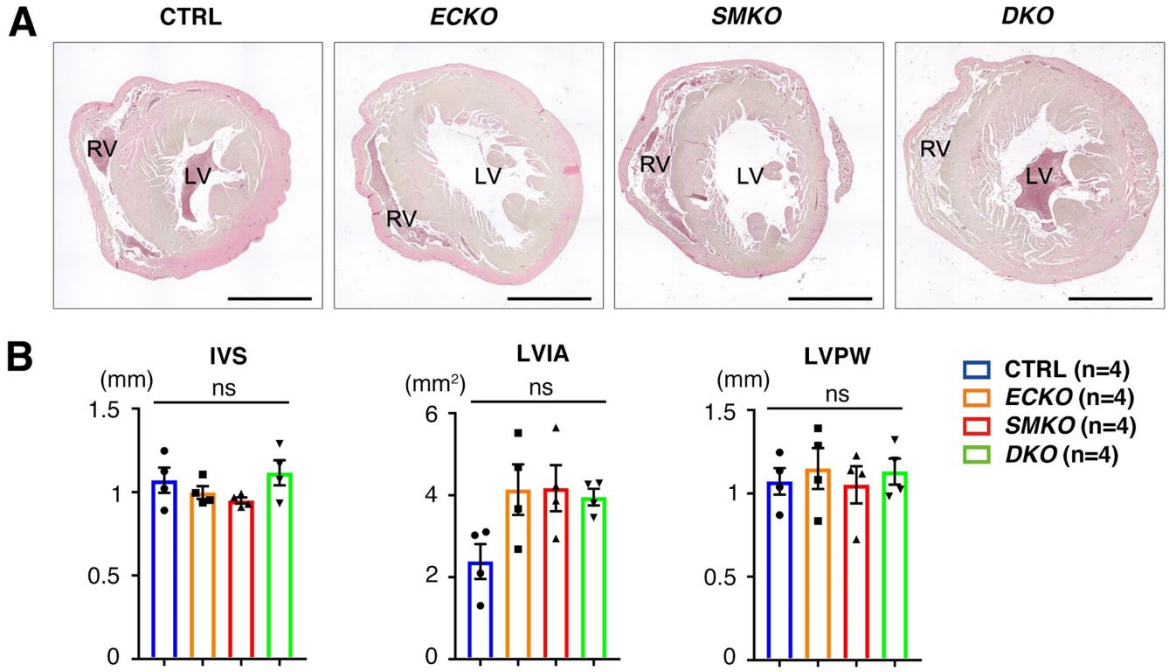

(**A**) Cross sections of heart from CTRL (n=4), ECKO (n=4), SMKO (n=4) and DKO (n=4) at postnatal day 60, stained with HE. LV, left ventricle; RV; right ventricle. Scale bars are 2 mm. (**B**) Quantification of interventricular septum (IVS), left ventricular internal area (LVIA) and left ventricular posterior wall (LVPW). Bars are means ±SEM. NS, not significant, one-way ANOVA.

Figure S5. Evaluation of cardiac hypertrophy and cardiac function at 4 months old.

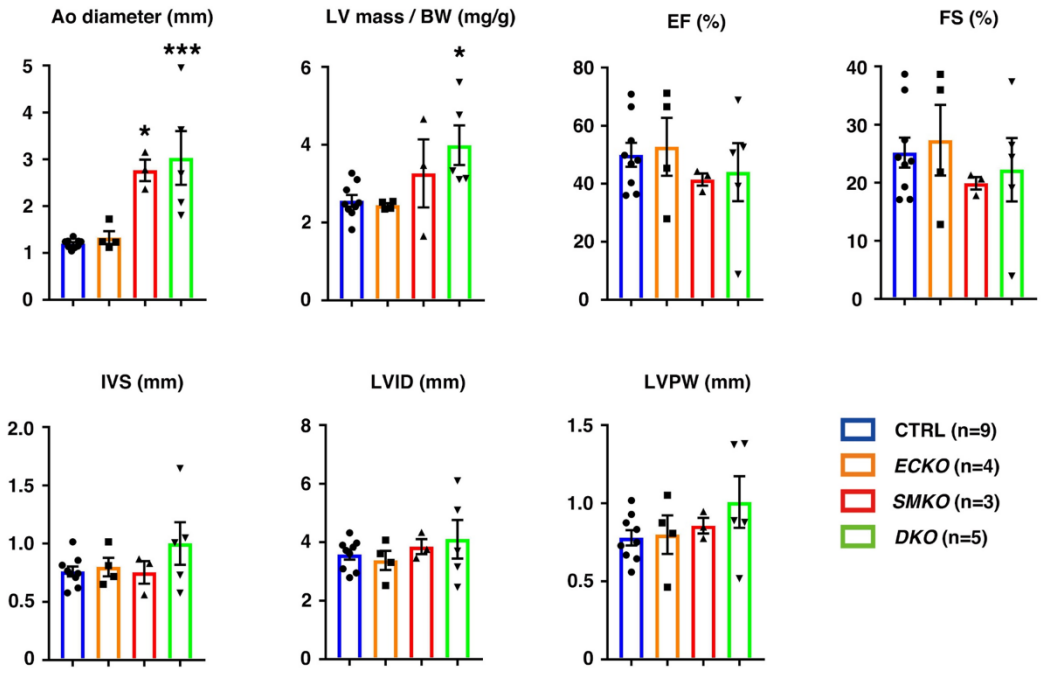

Quantification of outer aortic (Ao) diameter, left ventricle (LV) mass to body weight (BW), ejection fraction (EF), fractional shortening (FS), interventricular septum (IVS), left ventricular internal dimension (LVID) and left ventricular posterior wall (LVPW) in diastolic by echocardiography. CTRL (n=9), ECKO (n=4), SMKO (n=3), and DKO (n=5). Bars are means ± SEM. *P < 0.05, ***P < 0.001, one-way ANOVA.

Figure S6. Pulse wave doppler tracing of aortic valve at 2-month-old mice.

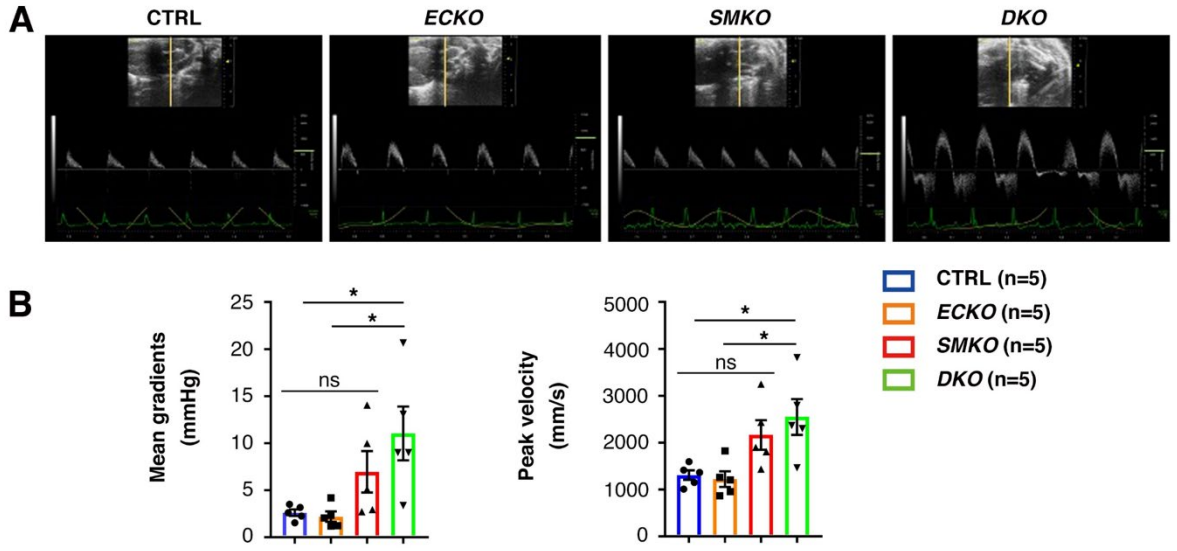

(**A**) Representative images of aortic transvalvular flow velocity by pulse wave doppler. Measurement points are indicated by yellow lines. Light green lines represent 1000 mm/s velocity and green curves indicate ECG. CTRL (n=5), ECKO (n=5), SMKO (n=5), and DKO (n=5). (**B**) Quantification of aortic transvalvular systolic mean gradients and aortic transvalvular peak velocity in A. Bars are means ± SEM. *P < 0.05. NS, not significant, one-way ANOVA, compared to CTRL and ECKO mice.

Figure S7. Evaluation of cardiac hypertrophy and valve thickness at postnatal day 14.

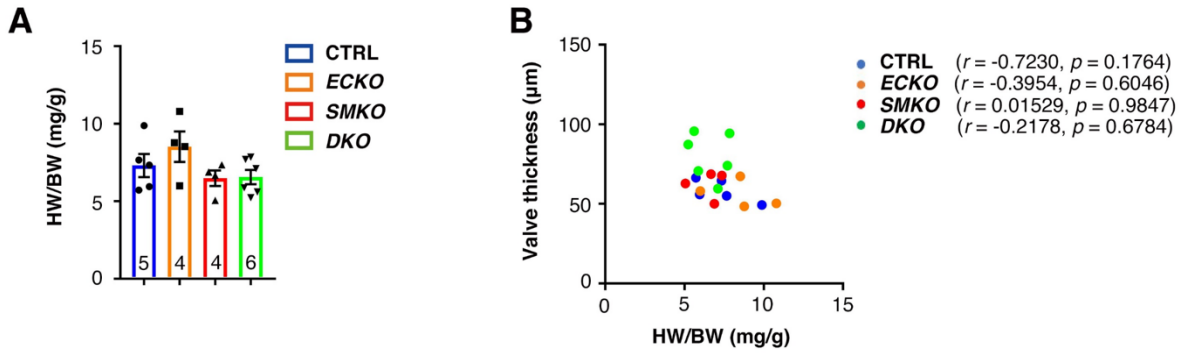

(**A**) Cardiac hypertrophy was evaluated by measuring heart weight to body weight ratio (HW/BW). CTRL (n=5), ECKO (n=4), SMKO (n=4) and DKO (n=6). Bars are means ± SEM, one-way ANOVA. (**B**) Correlation with HW/BW (in A) and valve thickness (shown in Figure 4). Pearson r shows correlation, where +1 is a total positive linear correlation, 0 is no linear correlation, and -1 is a total negative correlation. Two-tailed P value is also shown.

Figure S8. Morphological analysis of pulmonary valves, mitral valves and tricuspid valves.

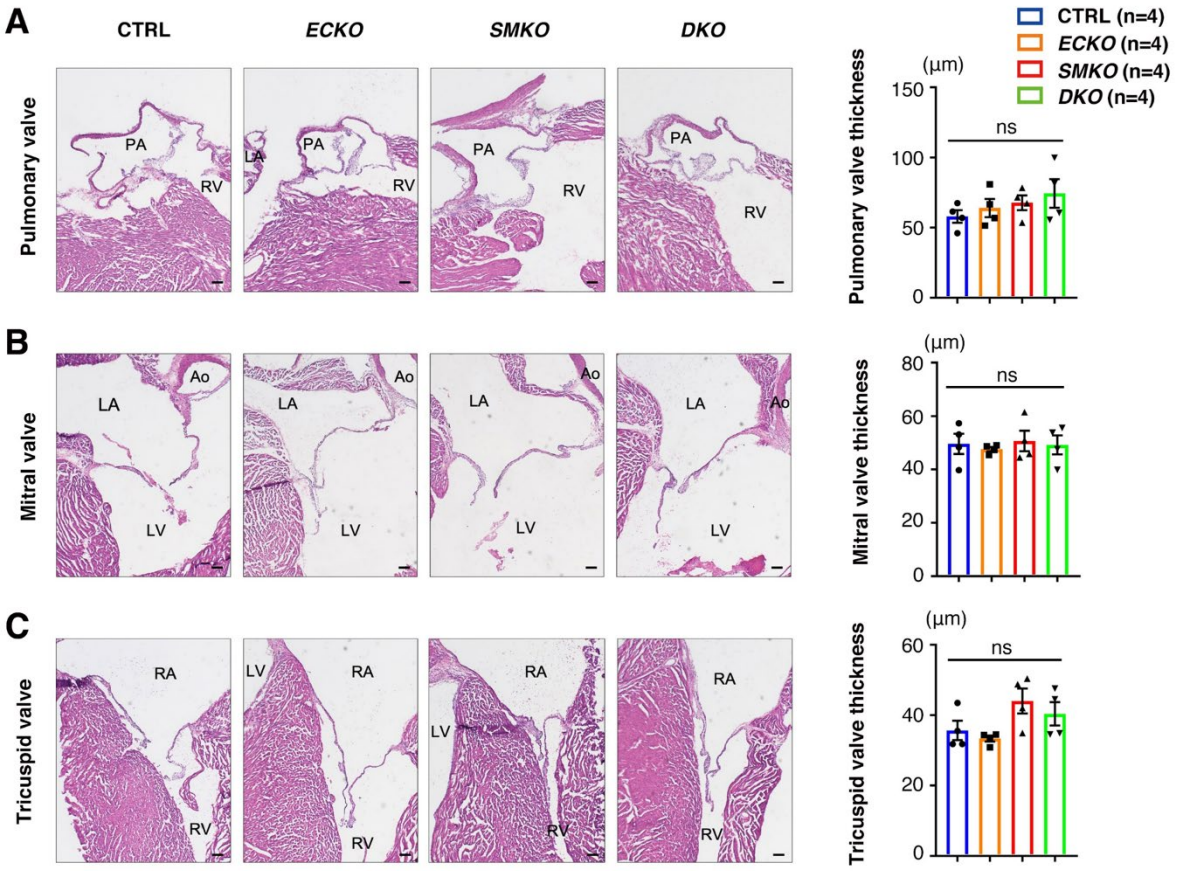

Histological images of pulmonary valve (**A**), mitral valve (**B**), tricuspid valve (**C**) from CTRL (n=4), ECKO (n=4), SMKO (n=4) and DKO (n=4) at posnatal day 60 stained with hematoxylin and eosin. PA, pulmonary aorta; RV, right ventricle; Ao, aorta; LA, left atrium; LV, left ventricle; RA, right atrium; RV; right ventricle. Scale bars are 100μm. Quantification of valve thickness is shown on the right. Bars are means ±SEM. NS; not significant, one-way ANOVA.

Figure S9. RNA-seq analysis of aortic valves.

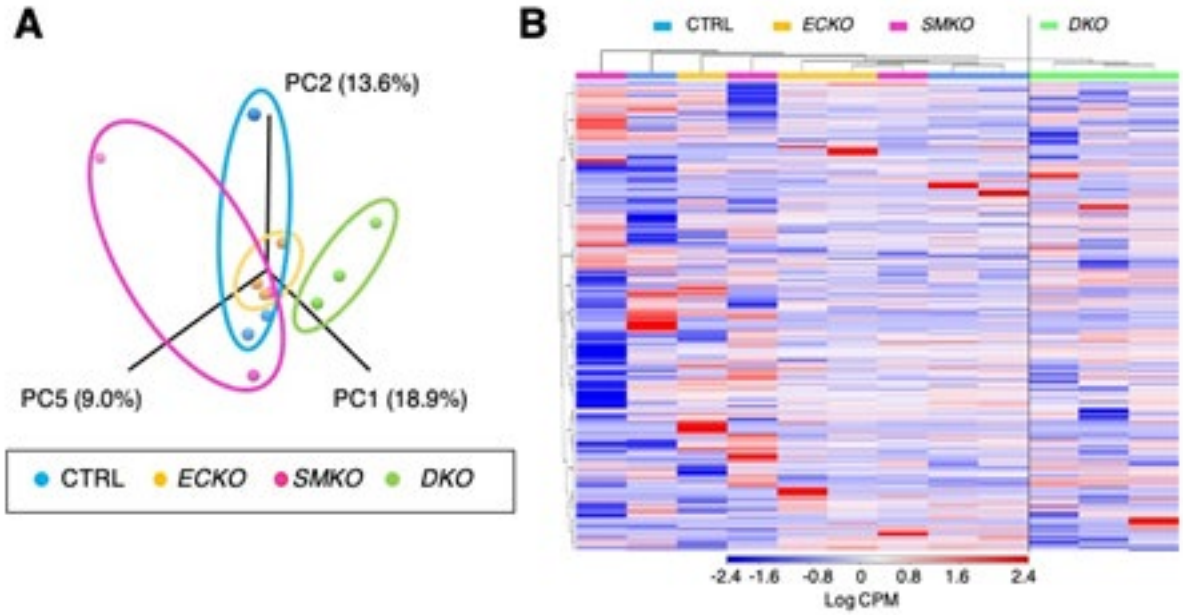

(**A**) Principal component analysis (PCA) plots show distinct groups according to the condition and genotype. PC1 (18.9%), PC2 (13.6%), and PC5 (9.0%). The DKO group does not overlap with the others. (**B**) Heat map showing the individual log counts per million (CPM) values of gene expression from 3 conditions per genotype. Hierarchal cluster showing DKO group separated by other groups.